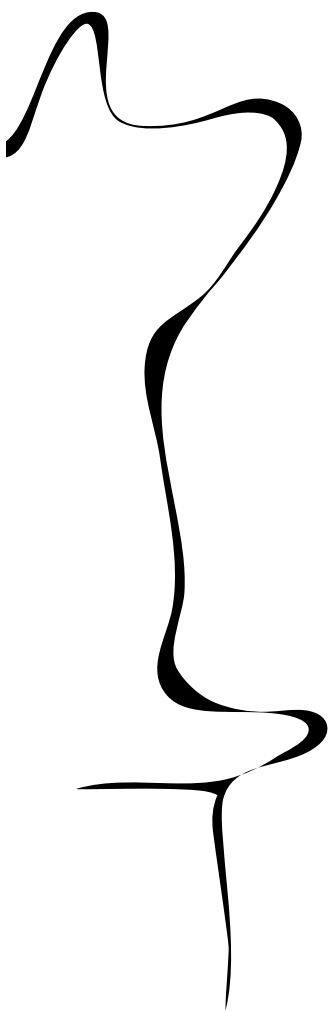


Engineering Technology (ET)

Design of an innovative natural ice skating rink

Mechanical Engineering
Faculty Engineering Technology

Michael Hop



Thesis supervisor: prof. dr. ir. G. Brem

Supervisor: ir. E.A. Bramer

February 8, 2021

UNIVERSITY OF TWENTE.

Contents

1	Introduction	1
1.1	Research objective	2
1.2	Organisation of the report	2
2	Literature study	3
2.1	Ice models	3
2.2	Surface energy budget	5
2.2.1	Ice growth	5
2.3	Conduction	5
2.3.1	Model of daily variations in soil temperature	6
2.3.2	Insulating materials used in road construction	8
2.3.3	Conclusion	9
2.3.4	Application Winterswijk	9
2.4	Convection	10
2.4.1	Flat plate	10
2.4.2	Atmospheric stability	10
2.4.3	Latent heat transfer	11
2.5	Radiation	13
2.5.1	Solar heat exchange	14
2.5.2	Short wave radiation	14
2.5.3	Long wave radiation	15
2.6	Conclusion	17
3	Ground isolation experiment	18
3.1	Intro	18
3.2	Estimation of insulation benefit	18
3.3	Method	19
3.4	Results	20
3.5	Discussion	21
3.6	Conclusion	21
4	Modelling ice growth on an ice skating rink	22
4.1	Finite volume method	22
4.1.1	Numerical instability	23
4.1.2	Interface resistance	24
4.1.3	Temperature and enthalpy	25
4.1.4	Enthalpy method	25
4.2	Turbulent energy flux	25
4.3	Longwave energy flux	26
4.4	Shortwave energy flux	26
4.4.1	Declination angle	27

4.4.2	Hour angle	27
4.4.3	Shortwave absorption and reflection	27
4.5	Calculation loop	28
5	Ice growth model validation and prediction	29
5.1	Verification	29
5.1.1	Ice floor layers	29
5.1.2	Model input parameters	30
5.1.3	Temperature profile	30
5.1.4	Discussion	32
5.2	Predictions	33
5.2.1	Difference between insulated and non-insulated configuration	33
5.2.2	Difference in temperature profile	33
5.2.3	Difference in ice growth	34
5.2.4	Effect of asphalt thickness	36
5.2.5	Effect of the water layer height	36
5.3	Discussion	37
5.4	Conclusion	38
6	Building ice by spraying layers of water	39
6.1	Basic nozzle dynamics	39
6.1.1	Cone nozzle	40
6.1.2	Flat jet	40
6.1.3	Recommendation Winterswijk	40
6.1.4	Nozzle flow rate	40
6.2	Theory spray droplet trajectory	41
6.2.1	Influence of gravity on the droplet trajectory	41
6.2.2	Drag	42
6.2.3	Max range of a nozzle	43
6.2.4	Water distribution of a nozzle	44
6.3	Design of 400m water spray cart	46
6.3.1	Ice rink challenges	46
6.3.2	Turn compensation	47
6.3.3	Redistributing the nozzle location	47
6.3.4	Total water flow rate	48
6.3.5	Water layer height	49
6.4	Final design	51
6.5	Conclusion	51
7	Ice growth via spraying of multiple water layers	52
7.1	Introduction	52
7.2	Hypothesis	52
7.3	Setup	53
7.4	Method	53
7.4.1	Ultrasonic pulse-echo method	54
7.4.2	Cold plate	54
7.4.3	Peristaltic pump	54
7.4.4	Temperature sensor	54
7.4.5	Final setup	54
7.5	Calculations	55
7.5.1	Heat transfer	55
7.5.2	Ice thickness	56

7.6	Results	58
7.7	Discussion	58
7.8	Conclusion	59
8	Discussion	61
9	Conclusion	64
A	Appendix ice growth rate experiment	68
A.1	Ice growth experiment sigmoid curves	68
B	Material properties	70
B.1	Thermo-physical properties of pavement materials	70
C	Spray cart design	71
C.1	Water layer height spray cart	71

Summary

Due to the effects of climate change fewer days of frost are measured during the winter[1]. This has limited the citizens of the Netherlands to perform one of their most iconic sports, ice skating. Based on the results of this study, a new innovative ice skating track has been constructed in Winterswijk which makes use of an insulating layer below the asphalt where the ice floor is built on. In addition, water spray carts are used to create an ice floor, allowing for more precise control of the ice growth process. This research has focused on the optimal design of an outdoor ice skating rink that can be used more often and during less severe winters. This has been established with the creation of an ice growth model, which allows for time-varying input conditions and incorporates a detailed heat transfer model for the underlying ground.

In addition to the ice growth model, two experimental setups have been constructed. The first experimental setup confirmed the effectiveness of insulation. With the help of a small-scale model of the ice rink floor, the asphalt temperature has been measured for the case with and without insulation. The results showed a difference of 2.5 Celsius in surface temperature for the insulated case at the end of the night compared to the non-insulated case. The reduced surface temperature demonstrated that ground flux is a significant factor for the energy surface balance, reducing the ground heat flux helps for more ice to grow. Furthermore, the ice growth model allowed to simulate the expected ice growth for a variety of ice rink floor configurations and ambient conditions. The data from the experimental setup has been used to verify this model. By replacing the mixed granulate subbase with foamed concrete, it is possible to achieve an ice layer of 12mm instead of 6.5mm at the end of a single night. Furthermore, the ice growth model showed that heat transfer by radiation is a significant factor in ice growth, with an effect of up to 0.7 mm per hour of ice growth in case of clear skies and an ambient temperature of zero degrees Celsius.

The conventional method of creating an ice layer is by flooding the ice track and waiting until a few centimetres of the top layer are frozen. After that, the water beneath the ice layer will be drained and the ice floor descend onto the asphalt. By using water spray carts, the water now always freezes at the top side of the ice, allowing for faster ice growth and more precise control of the ice thickness. Results from the ice growth model showed that the timing of a new water layer is important. A new layer should be applied before the last layer is completely frozen for a faster rate of ice growth. To sustain an even distribution of water over the track the nozzles have been moved to compensate for the longer distance of the outer edge.

The second experimental setup concerns the ice growth experiment. This experiment investigates the effect of the water layer height on the freezing rate. The pulse echo method was used to measure the ice thickness without interfering with the ice growth process. However, the sensor data from this method proved to be unreliable. Therefore, no conclusions could be drawn from this experiment about the effect of water layer height on the freezing rate.

The result of this study is that the ice skating rink in Winterswijk now uses spray carts to form an ice layer and has placed foamed concrete as an insulating layer, which has proved to be successful during the night of November 30 in 2020. Ice skating was already possible after a single night of frost [2][3].

Chapter 1

Introduction

It is no secret that the Dutch love to ice skate. The performance of the Dutch speed skaters at the Winter Olympics is one aspect that shows this. One of the reasons is the topography of the Netherlands, the flat land with water canals throughout the country. During cold winters these canals freeze over giving the opportunity for residence to go ice skating nearby. One of the main ice skating events in the Netherlands is the Elfstedentocht (Eleven cities tour) long-distance tour skating event reaching almost 200 kilometres long. The first official ice skating race was organised in 1909 and since then has only been organised 14 times with the last tour in 1997. For the eleven cities tour, an ice thickness of 15 centimetres is necessary to sustain the great number of ice skaters. Research data from the KNMI showed that for a continuous cold period of fifteen days with an average temperature of below -4.2°C it is very likely for an eleven cities tour[1]. Due to global warming, the chance of an eleven cities tour happening has been steadily decreasing from once in four years during 1950 to once in sixteen years in 2020. In addition to the possibility of skating on canals, the Netherlands also has many natural ice skating rinks throughout the country, varying from a simple grass field flooded with water to a full fledged 400m ice skating track. During each winter, ice skating associations throughout the Netherlands compete to host the first ice skating marathon on natural ice. Several unique ideas are used around the country to decrease the time it takes to grow a layer of ice, varying from spraying the track with a slurry tank behind a tractor or placing sun screens to reduce melting during sunny days. The competing ice skating associations for the first marathon are located in Noordlaren, Veenoord, and Haaksbergen. A new addition to this list might be Winterswijk as the ice skating association in Winterswijk constructs a new ice skating rink. Coincidentally, Winterswijk holds the record for the coldest night, with a temperature of -27.4°C in the year 1942. The construction of the new ice skating rink in Winterswijk is the starting point for this research. This research will focus on getting a better understanding of the ice growth process on natural ice skating facilities and apply this knowledge in Winterswijk in the design of the ice skating rink. This will allow the ice skating association of Winterswijk (WIJV) to make better use of the facility and increase the chances of having an ice floor. Research aspects that will be investigated are the possible benefits of placing an insulating layer below the ice, to prevent conduction from the warm ground. Additionally, the WIJV will construct a spray cart which will apply layers of water instead of the conventional method of flooding the ice rink. This in turn allows for more flexibility during the creation of an ice layer.

1.1 Research objective

The main research question of this research, which is as follows: "In what way can the design of a natural ice skating rink be improved to increase the potential use?". To be able to answer this question, the main factors influencing ice growth and melt are investigated and a theoretical model for ice growth is formed. The theoretical model itself allows for the analysis of the important conditions for ice growth and the model itself is verified by an experimental setup. Other research sub questions focus more on the spraying of water and design of the spray cart built by the WIJV. Finally, all this together leads to the design of an optimal natural ice skating rink, giving the upper hand to the WIJV.

What are the key factors influencing ice growth and melt?

What is the optimal design of an isolated ice skating floor?

What is the most optimal nozzle configuration for spraying water on the ice skating rink?

What is the effect of the sprayed water layer height on the ice growth rate?

1.2 Organisation of the report

The report starts with a study about ice growth models used in the literature and the varying energy fluxes involved with either growing or melting of ice in open air. The relations found in literature are combined to create a model in chapter 3. This ice growth model is able to calculate the expected ice growth based on meteorological parameters. An experimental setup has been designed and built at the University of Twente, which is discussed in detail in chapter 4 and the results are used in chapter 5 as verification for the ice growth model. Chapter 6 describes the design of the spray cart used in Winterswijk and the placement and selection criteria for the used water nozzles. Chapter 6 describes the experimental setup in the lab, which is used to obtain the relationship between ice growth rate and water layer height. Chapter 7 discusses the results of the entire research and proposes recommendations for future research. The final chapter concludes the findings of the report.

Chapter 2

Literature study

This chapter will discuss the findings from the literature about ice growth on natural ice. The first section discusses a variety of ice models and relations used to estimate the ice growth on open water. The limitations of these models are discussed and show the need for a new enhanced model focused for ice growth on an ice skating rink. Each section afterwards focuses on a different mode of heat transfer during ice growth on an ice skating rink. These different modes are: conduction, convection and radiation. The findings of this chapter are used as the starting point for the ice growth model in the next chapter and allow for answering the first sub question: What are the key factors influencing ice growth and melt?

2.1 Ice models

There are many meteorological variables that play a role in the growth of an ice layer, which makes it an interesting problem to model. In addition to this, water has its highest density at 4° and this causes water with a temperature below 4° to rise to the surface. Allowing ice to form on the top surface while water further below the surface is still a few degrees above the freezing point. Further cooling will result in ice formation at the surface growing downwards. Wind can be an important factor to transfer cold or warm air by convection to the ice or generate turbulence in the water layer which enhances the mixing of water resulting in an increase of the surface temperature. This is due to the fact that warmer water on the bottom can mix with the colder water on top. One aspects of ice growth is the radiation balance, which is often visible in practice. For example, ice under a bridge is not able to discard heat via radiation to the night sky, preventing it from freezing over or locally reducing the ice thickness.

In the Netherlands, Bruin and Wessels designed an ice growth model which is used by the Royal Netherlands Meteorological Institute (KNMI) [4]. The model is used for forecasting the thickness of a layer of ice one week in advance in the range of 0 to 20 cm of ice. The model includes the situation of ice with a snow cover and pays special attention to the optimal estimation of the net radiation and the role of the stability of the surface air. The work, of Keijman (1974) was used by Bruin and Wessels which investigated the energy balance of a lake [5]. In this work a relation is presented to estimate the net long wave radiation, which incorporates the cloud coverage. According to the research of Ashton (1989) the most commonly used method for predicting ice thickness is based on the "Stefan problem", which describes the temperature distribution in a homogeneous medium undergoing a phase change [6]. The Stefan problem is greatly simplified, the top surface temperature is fixed and the heat flux through the ice is expressed in the form below:

$$Q_i = -k(T_m - T_s)/h \quad (2.1.1)$$

where Q_i is the heat flux through the ice, k is the thermal conductivity of the ice, h is the thickness, T_m the temperature of the water-ice interface (0°C) and T_s the temperature of the top surface. This heat flux is balanced at the bottom surface by the production of ice at a rate:

$$\rho\Delta H_{fus}dh/dt = Q_i \quad (2.1.2)$$

where ΔH_{fus} is the enthalpy of fusion, ρ the density of ice, and t is time. Combining both equations and integrating with the initial conditions that $h = 0$ and $t = 0$ results in:

$$h = \left(\frac{2k}{\rho\Delta H_{fus}} \right)^{1/2} [(T_m - T_s) t]^{1/2} \quad (2.1.3)$$

In equation 2.1.3 the bracketed term is the "square root of freezing days", this relation is often used as a crude method to estimate ice thickness. This relation only holds if the top surface temperature is equal to the air temperature. However, data shows that an additional coefficient, usually in the range of 0.5-0.8, is needed to obtain accurate results. Generally, the measurements for the coefficient are taken with an ice thickness larger than 10 cm, which is outside the range of ice thickness commonly seen in the Netherlands. In the model, the effect of specific heat is neglected and the assumption is made that the top surface has the same temperature as the ambient air. In the model of George D. Ashton, he expressed the flux of heat from the ice surface to the air with the bulk heat transfer coefficient h_{bulk} and the temperature difference between the ice and air as stated in equation 2.1.4 [6].

$$Q_{ia} \equiv h_{bulk} (T_s - T_a) \quad (2.1.4)$$

This relation showed to be more accurate for thin ice growth. The bulk heat transfer coefficient is set as a constant value with consideration of the wind speed. Still air conditions showed that h_{bulk} is in the neighbourhood of $10 \text{ W m}^{-2} \text{ }^\circ\text{C}^{-1}$, for conditions typical for mid-western United States a value of $20\text{-}25 \text{ W m}^{-2} \text{ }^\circ\text{C}^{-1}$ has been found to be reasonable. In exposed and windy conditions, a value as high as $30 \text{ W m}^{-2} \text{ }^\circ\text{C}^{-1}$ has been accurate if the ice growth holds on for several days. Another study performed by Fang (1996), produced an algorithm for ice formation on a lake and tested this for a lake in Minnesota [7], the research focused on the freeze-over moment of the lake. A study performed by Launiainen and Cheng produced a model valid for sea ice and paid additional attention to the short-wave radiation extinction in ice and snow [8], this showed to be important for sunny days. In this study, the effects of saline water will not be taken into account because the ice skating rink will only use fresh water.

While there are enough models available for estimating ice growth on lakes and rivers, limited research is done on ice growth on a natural ice skating rink. Especially, heat conduction through the ice rink floor is not studied in detail. The models used in the literature use large steps in time and space, thereby reducing the accuracy for short-term estimations. This study aims to create a model that is valid for natural ice skating rinks with high spatial resolution and with the inclusion of a ground heat transfer model. This is to fill the gap in the literature on ice growth models for ice skating rinks. In the next section a closer look is taken into the required time to obtain an ice layer and the individual modes of heat transfer.

2.2 Surface energy budget

The surface heat transfer controls the growth rate of ice. Therefore an accurate estimate of the surface heat flux is needed. The surface exchanges heat with the atmosphere through five different modes of heat transfer. These are; shortwave solar radiation Q_{SW} , atmospheric downward long-wave radiation $QLW \downarrow$, upward long-wave radiation from the ice surface $QLW \uparrow$, conduction Q_{cond} , sensible Q_s , and latent heat Q_l often combined into one term. While precipitation can be of influence on the energy budget of an surface, for the sake of simplicity, this is left out.

2.2.1 Ice growth

The ice growth rate depends on the net heat flux and the starting temperature of water. However, the sensible heat part of the water layer has only minimal impact on the total growth rate of ice. The energy needed to extract out of a layer of water to completely freeze the ice, is given by equation 2.2.1 with m the mass of water C_p the specific heat of water, T_i and $T_{freezing}$ the initial temperature of the water and freezing temperature of ice respectively and last the heat of fusion ΔH_{fus} .

$$E = mC_{p,water}(T_i - T_{freezing}) + m\Delta H_{fus} \quad (2.2.1)$$

Knowing the heat flux leaving the layer of water and combining this with the density of water to rewrite the mass to a specific layer height. The time till freezing can be calculated for different circumstances, as is illustrated in figure 2.1. With time until frozen on the x-axis and the layer height on y-axis. The initial temperature of the water is set to 10 °C. To obtain a freezing rate of 1 mm/h, a heat flux of 104 W m⁻² is necessary. In the case of water with a starting temperature of 0 °C a energy flux of 92 W m⁻². The difference in heat flux shows that the majority of the extracted energy is used for the phase transition. With this in mind, it is now possible to estimate the ice growth rate from a basic standpoint.

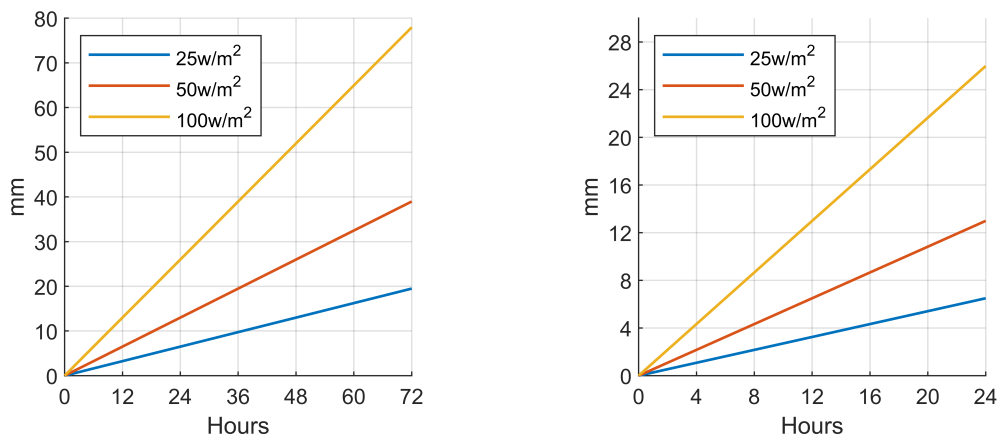


Figure 2.1: Time until frozen against the layer height for large and small layer heights.

2.3 Conduction

In the ice growth model of lake, conduction is only through the ice layer. In the case of ice on an asphalt ice skating rink the ground transfers heat to the ice by conduction. This section will discuss conduction in the ice rink floor with a focus on heat transfer through soil. In soil without any movement of either water or gas, the vertical flux of heat q_{cond} (W m⁻²) is described by Fourier's law:

$$q_{cond} = -k \frac{\delta T}{\delta x} \quad (2.3.1)$$

Equation 2.3.1 relates the energy flux in the soil layer to the thermal conductivity k ($\text{W m}^{-1} \text{K}$) and the gradient in temperature T (K) over a distance x . While the thermal conductivity is observed as an independent factor, it should be considered as apparent soil thermal conductivity, since the total heat flux in soil exists not only out of conduction but also from the movement of water in both the vapour and liquid states. The movement of moisture in the soil by evaporation and subsequent condensation due to a temperature gradient can alter the total heat flux. Therefore, moist soils have coupled heat and mass transfer equations. In the case of a natural ice skating rink, the surface layer is made from asphalt and not permeable by water. Extensive analysis of the effect of water vapour diffusion is therefore left out in this research. The thermal conductivity of soil is made up by the porosity of the soil, the water content, and the composition of minerals in the soil. Conductivity of the different components in soil also varies greatly, quartz has a conductivity of $1.46 \text{ W m}^{-1} \text{K}$ while for example, air has a thermal conductivity of $0.0262 \text{ W m}^{-1} \text{K}$ [9]. In dry soil, the limited contact points between mineral particles reduce the contact area thereby reducing the heat transfer. Water can act as a bridge between the mineral particles and so influences the thermal conductivity to a great extent. This effect is especially noticeable at lower water content. Thermophysical properties of several common ground materials are shown in table B.1 in the Appendix. The heat capacity per unit volume of soil is the amount of heat required to raise the temperature of the unit volume by one degree Kelvin. With knowledge of the volume fractions ϕ of the soil constituents, specific heat per unit mass and densities, the specific heat per unit volume can be calculated by using equation 2.3.2.

$$c_v = \sum_i \rho_i \phi_i c_i \quad (2.3.2)$$

The heat capacity of the soil is important since a layer of material with a high specific heat capacity and low thermal conductivity is able store energy for a long time. Its common to describe this with thermal diffusivity. The thermal diffusivity is the ratio of thermal conductivity to the volumetric heat capacity $\alpha = \frac{k}{C_v}$. High thermal diffusivity means that the material can change rapidly in temperature and low thermal diffusivity means that the material takes longer to change in temperature. Again, water content is important when it comes to the thermal diffusivity, since the heat capacity changes linearly with the water content while the thermal conductivity increases rapidly at lower water contents.

2.3.1 Model of daily variations in soil temperature

The periodic changes of temperature in the soil are studied in soil thermal regime. The periodic changes of atmospheric conditions control the in and outflow of energy at the surface and can either be diurnal (daily) or yearly. These cycles serve as a baseline, however due to the irregularities in meteorological events such as cloudiness, warm and cold fronts, precipitation, the soil temperature does not follow this cycle completely. As heat travels downwards through the soil, the energy flux is used to raise the soil temperature. As a result of this a decrease in energy flux is seen with depth. This observation can be modelled as amplitude damping, a reduction of the temperature amplitude with depth. If the surface temperature ($z=0$) is considered purely harmonic over time, with a mean value of T and amplitude of A_0 the following equation holds for the surface temperature.

$$T(0, t) = T + A_0 \sin \omega t \quad (2.3.3)$$

Incorporating the decay of temperature, which is a function of depth, into equation 2.3.3 gives equation 2.3.4. The depth(z) below the surface is expressed as a positive number. The t_{offset} is the offset as to obtain the maximum surface temperature at 15:00, which is consistent with many field measurements [10]. This offset value can be modified to be consistent with the measured temperatures and obtain the optimal agreement. Temperature profile of the ground is plotted in figure 2.2 with a mean temperature of 0°C and amplitude of 10°C , the soil is simulated as mixed granulate. The figure clearly shows the dampening effect and the lag between maximum and minimum temperature at different depth levels. The significance of this dampening and lagging is the fact that the surface temperature could reach 0°C while the ground below is still warm thereby melting a layer of ice later.

$$T(z, t) = T + A_0 \exp^{-d/z} \sin \left[\omega(t - t_{offset}) - \frac{z}{d} \right] \quad (2.3.4)$$

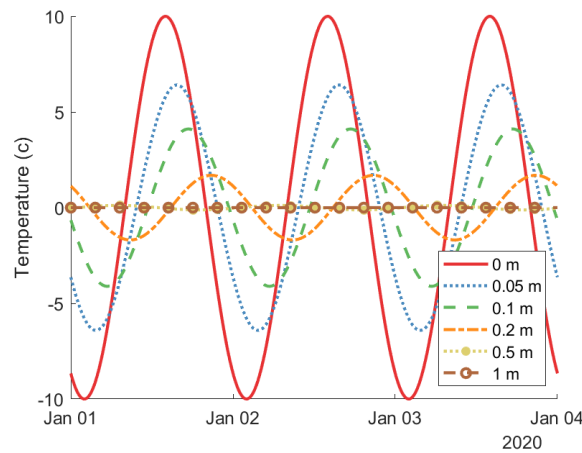


Figure 2.2: Temperature profile at various depths in standard crushed gravel with a thermal diffusivity of $4.6 \times 10^{-7} \text{ m}^2 \text{ s}^{-1}$

The last parameter is the characteristic damping depth described in equation 2.3.5, which is the depth at which the amplitude is decreased to the fraction $1/e$ of the surface amplitude.

$$d = \sqrt{2D_H/\omega} \quad (2.3.5)$$

Local soil measurements with time and depth coupled with the above solution can be used to obtain soil thermal properties. Two commonly used methods are the phase lag method and amplitude ratio method. The first method uses the difference in time (phase lag) between the peaks in maximum temperature at two different depths. The other method makes use of the ratio of two amplitudes measured at different depths. Research showed that the phase lag method was more reliable compared to the amplitude ratio method especially further below the surface where the amplitude change is small [10]. The amplitude method relation is shown in equation 2.3.6, and allows for estimating the soil measurements without destroying the soil layers.

$$D = \frac{\pi}{\tau} \left(\frac{z_2 - z_1}{\ln(A_1/A_2)} \right)^2 \quad (2.3.6)$$

2.3.2 Insulating materials used in road construction

The aim of this section is to make a selection of insulating materials used in road construction which could be used in Winterswijk. At the end of the section, the material and configuration used in Winterswijk is presented. A road is a structure consisting of several layers on top of the natural soil. The natural material on which the entire road structure rests is called subgrade and is the compacted material on-site. On top of the subgrade, four distinct layers are commonly placed: subbase layer, base layer, binder layer, and surface layer. The subbase layer has the primary function to provide structural support and improve drainage. A subbase layer is not always needed or used in practice if the subgrade is sufficiently stiff. In Winterswijk, a subbase layer is not necessary. The base layer provides additional load distribution and is often composed of a mixture of granulate materials of crushed stones and slag. An insulating material would be used as replacement for the base layer. On top of the base layer rests the binder layer which exists of an open graded mixture of asphalt with reduced quality compared to the surface layer. The surface layer is in direct contact with traffic loads and is generally constructed with dense graded asphalt. The surface layer must provide a smooth surface and adequate water drainage and be water proof. Water proofing is especially important for the current use case as a basement for an ice rink. Insulating roads to achieve a colder surface temperature is not a common practice, therefore limited research is available about the effect of replacing a layer with an material that insulating properties. Research in Norway[11] tested three different insulating materials for road construction as a method to avoid freezing of the subbase layer. The three different materials tested are: lightweight clay aggregate(LWCA), foam glass aggregate, and extruded polystyrene boards (XPS). An additional material also discussed in this section is foamed concrete. The four different materials are each discussed below. The selected material would replace the base layer, which exists of mixed granulate with an thermal conductivity of $1.1 \text{ W m}^{-1} \text{ K}$ and a density of 2190 kg m^{-3} .

Lightweight clay aggregate (LWCA) is used as lightweight fill or frost protection in road construction. The fabrication of lightweight clay aggregate happens in special furnaces by sintering clay. Density of the material varies from $250 \frac{\text{kg}}{\text{m}^3}$ to $500 \frac{\text{kg}}{\text{m}^3}$ [12]. Characteristics of the material are the low thermal conductivity coefficient $0.097 \frac{\text{W K}}{\text{m}}$ [12]. Water has the ability to pass through the layer of lightweight clay aggregate, thereby increasing the thermal conductivity and reducing the net effect of insulation.

Foam glass aggregate is produced by recycling waste glass. It can be produced in various densities, the typical bulk density is in the range of $180 \frac{\text{kg}}{\text{m}^3}$ to $250 \frac{\text{kg}}{\text{m}^3}$. Moisture content of the foam glass was found to be around 20 % by weight (6% by volume) corresponding to a thermal conductivity of $0.155 \frac{\text{W K}}{\text{m}}$ at a temperature of 10°C . The thermal conductivity of foam glass can vary significantly with temperature and water content [11].

Extruded polystyrene or XPS insulation is manufactured through an extrusion process. During this process, the ingredients of XPS melt together and are continuously extruded through a die to form closed cell insulation. This has the added benefit that water is unable to penetrate the XPS, which is not the case with normal expanded polystyrene (EPS). Additional benefit is that water is unable to penetrate into the layer, thereby changing the thermo physical properties of the material negatively. Density of XPS is about $50 \frac{\text{kg}}{\text{m}^3}$ and the thermal conductivity is only $0.04 \frac{\text{W K}}{\text{m}}$. The major downside of using XPS is the fact that it is not possible to lay asphalt directly on XPS as the asphalt would melt the material during construction. If XPS is used in road construction it is therefore placed below the base layer, this greatly reduces the effectiveness of preventing heat transfer to the surface.

Foamed concrete is the last material discussed and typically consists of a slurry of cement, sand, and water with a foaming agent. A slurry of cement and water is used for lightweight mixes. The slurry is created by mixing the slurry intensively with water and air on site, this reduces the necessary trucks to deliver the materials to the building site. Allowing for a more environmental production of

roads. The density of foamed concrete varies between 200 kg m^{-3} to 1600 kg m^{-3} . The end product consists of large cavities of air which improves the thermal performance as an insulator, lightweight foamed concrete can have a thermal conductivity of only $0.03 \frac{\text{W}}{\text{mK}}$. Foamed concrete is available both as permeable and non-permeable to water. The non-permeable type would be preferred, as this eliminates the increase in thermal conductivity when water content increases and eliminates the ability of water vapour to transfer heat through the material.

2.3.3 Conclusion

Transfer of heat by conduction to the underlying ground varies with the used road construction material. The thermal conductivity of insulating materials is up to 30 times lower compared to the thermal conductivity of mixed granulate. In addition to a decrease in thermal conductivity the materials also have a reduced density, limiting the ability to store energy for a longer period of time. The reduced ability to store thermal energy in the ground could provide the ability to create an ice floor earlier in the winter. The effect of a reduced ability to store energy is further investigated based on the results of the ice growth model in chapter 5. An increase in water content resulted in both an increase in thermal conductivity and heat capacity, a sharp increase in thermal conductivity is seen due to the formation of water bridges between the material particles. This in turn could negatively influence the ability to create an ice floor. The effect of heat transfer from the ground to the ice layer is not to be underestimated and a more in detail approach is necessary to come to a conclusion to the effects it has on ice growth. A more detailed approach to showing the effects of ground heat transfer is made using the ice growth model.

2.3.4 Application Winterswijk

The ice skating rink in Winterswijk has chosen to construct the road with an insulating layer of foamed concrete. The layer of foamed concrete replaces the base layer of mixed granulate, thereby lowering the thermal conductivity and density of the layer. The type of foamed concrete used has an density of 600 kg m^{-3} and thermal conductivity of $0.1 \text{ W m}^{-1} \text{ K}^{-1}$ compared to 2190 kg m^{-3} and $1.1 \text{ W m}^{-1} \text{ K}^{-1}$ for mixed granulate. The foamed concrete layer has a thickness of 0.2 m, the binder layer has a thickness of 0.04m built with open grade asphalt and the surface layer has an thickness of 0.05m with dense graded asphalt.

2.4 Convection

Convection is the mechanism of heat transfer through a fluid in the presence of bulk motion. In the case of a ice growth on a asphalt layer this is the heat transfer from surrounding air to the ice when melting, and vice versa when freezing. The rate of convection is expressed by Newton's law of cooling in equation 2.4.1. The heat transfer coefficient h is strongly dependent on the fluid properties, shape of the surface and type of fluid flow.

$$Q_{\text{conv}} = hA(T_s - T_\infty) \quad (2.4.1)$$

2.4.1 Flat plate

Forced convection over a flat plate assumes that the velocity of the fluid at the surface is zero, the so called no-slip condition. As a result the heat transfer from the surface to the fluid layer is by conduction only since the fluid itself is motionless. As a result the convection heat transfer coefficient for a surface is varies along the flow direction and should be properly averaged to estimate the global heat transfer loss. It's common practice to non-dimensional the equation and combine the variable to into dimensionless numbers. Using the empirical relationship for the Nusselt number over a flat plat seen in equation 2.4.2 allows to calculate the heat transfer rate with 2.4.3 where k is thermal conductivity and L the characteristic length. The characteristic length for a plate is defined with the area divided by the perimeter $L = A/P$.

$$Nu = 0.037Re^{0.8}Pr^{1/3} \quad (2.4.2)$$

$$h = \frac{Nuk}{L} \quad (2.4.3)$$

For an example with typical freezing conditions($T_a = -6$, $T_s = -2$ and $u_10 = 3 \text{ m s}^{-1}$ the heat transfer coefficient is $20.3 \text{ W m}^{-2} \text{ K}$ and the total heat transfer 81.3 W m^{-2} . The Reynolds number depends on the velocity of the wind, characteristic length and dynamic viscosity shown in equation 2.4.4. Combining equations 2.4.2, 2.4.3 and 2.4.4 result in a relation for the heat transfer coefficient. While in normal circumstances in a lab it is possible to choose the correct characteristic length. This is not so easy for a heat transfer model of an ice rink. Taken the characteristic length of a square meter results in $L = 0.25$ while taking the width of the track results in $L = 2.5$ and thus a decrease in heat transfer coefficient of $10^{0.2} = 1.58$. Therefore, an empirical relation from literature focussed on surface heat transfer might be more suitable to use.

$$Re = \frac{uL}{\mu} \quad (2.4.4)$$

$$h = \frac{0.037(\frac{u}{\mu})^{0.8}Pr^{1/3}}{L^{0.2}} \quad (2.4.5)$$

2.4.2 Atmospheric stability

Thus far the stability of the atmosphere has not been taken into account. This is the effect of warmer air rising and colder air descending creating turbulence in the air. Under stable conditions, the surface temperature T_s is below the ambient temperature T_a and with unstable circumstances $T_s > T_a$. At the moment of ice growth the surface temperature is near freezing and thus unstable $T_a > T_s$ which in turn results in higher heat transfer rate. On the other hand during melting stage the conditions will be stable since $T_a > T_s$. The ambient temperature changes are considerable

and thus the stability effects should be taken into account. The Monin-Obukhov similarity theory describes the flow in the surface layer under non-neutral conditions as function of the Obukhov length, which is in turn related to the friction velocity and the sensible and latent heat flux. For practical calculations, solving the stability functions is too complicated, the functions are also very sensitive to relative small disturbances at the surface. The model of Bruin and Wessels searched for an empirical relationship and found the equations 4.2.1 and 4.2.2 in which the stability effects are incorporated. Using the same typical conditions as used in 2.4.5 results in $h = 7.5 \text{ W m}^{-2} \text{ K}$ for the stable conditions and $17.5 \text{ W m}^{-2} \text{ K}$ for the unstable conditions. This shows that a stability corrections is important for the ice-growth computation. Also the heat transfer from air to ice is larger when freezing compared to the same temperature difference when thawing. In the case of ice growing on a lake the the surface temperature needs to be below the freezing point and this could result in the atmospheric layer being stable instead of unstable. Resulting in a lower exchange of energy compared to the case where water is sprayed on top of the ice layer resulting in a surface temperature of zero Celsius and possibly a unstable atmospheric layer. Both relations are shown in figure 2.3 and figure 2.4.

$$h = 2.5U_{10} \quad T_s \leq T_a \quad (2.4.6)$$

$$h = 2.5U_{10} \left[\frac{1 + 10(T_s - T_a)}{U_{10}^2} \right]^{1/2} \quad T_s > T_a \quad (2.4.7)$$

2.4.3 Latent heat transfer

The latent heat due to evaporation and sublimation at the surface is proportional to the water vapour gradient. As for sensible heat the effect of latent heat is negligible without wind, as the boundary layer will soon be saturated and no further net evaporation from the ice surface can occur. A typical parameterization used is shown in equation 2.4.8 with k_{lat} the latent heat exchange coefficient and L_{lat} is the latent heat of sublimation. While this allows to calculate the latent heat transfer the heat exchange coefficient is complex and suffers from unstable and stable atmospheric conditions. In addition to this the energy related to evaporation or condensation of water vapour is the lowest contributor to the total energy balance. Therefore the relations from Bruin and Wessels are used described in the previous section which incorporates the latent heat transfer.

$$Q_{latent} = U \rho k_{lat} L_{lat} (w_a - w_s) \quad (2.4.8)$$

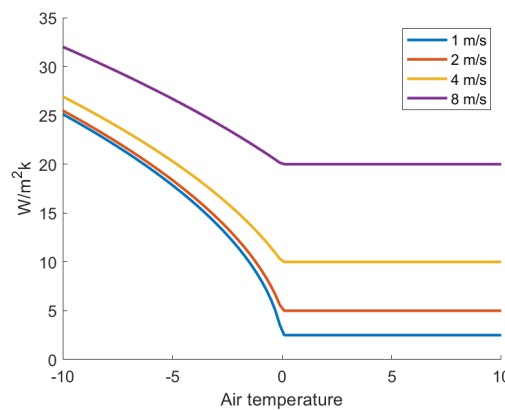


Figure 2.3: Heat transfer coefficient based on equation 4.2.1 and 4.2.2.

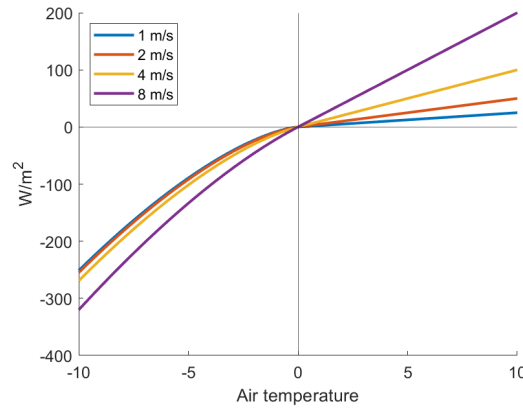


Figure 2.4: Heat transfer rate via convection with a surface temperature of 0 °C.

Heat transfer by sensible heat and latent heat are lumped together in the relation seen in equations 4.2.1 and 4.2.2. The resulting heat transfer varies widely with the ambient temperature but is in the range of $0 \text{ W m}^{-2} \text{ K}$ to $50 \text{ W m}^{-2} \text{ K}$. The total portion of energy subtracted by convection will be determined by the wind speed, as this has an enormous effect on the net heat transfer. Further research into the wind speed at night might be necessary for correct estimation. Research at Cabauw in the Netherlands[13] showed an decrease in air velocity during night time. The combination of an heat transfer model for the ground will provide accurate surface temperature allowing to see the full effect convection has on the heat transfer. It is expected that heat transfer by convection will on play a significant role when the temperature difference is significant. To achieve a significant difference in temperature, the ambient air temperature needs to be several degrees below the freezing point of water. The total heat transfer is also influenced by the atmospheric stability, therefore a stability correction is used in the relation. Due to this correction, the heat transfer coefficient is larger during ice growth and smaller during melting of the ice.

2.5 Radiation

This section will discuss the different forms of radiation heat transfer that play a role in the growth and melt of an ice floor. Heat transfer by radiation can be divided into two main types of radiation, namely short and longwave radiation. The first part of this section will focus on the different regions of radiation and shortwave radiation, the later part will focus on longwave radiation.

The total heat transfer via radiation of a surface is described by the incoming solar radiation and outgoing thermal radiation in literature net radiation is calculated by determining the incoming and outgoing shortwave radiation, respectively K^+ and K^- . The incoming and outgoing long wave radiation are described by L^+ and L^- . Calculating the net radiation effect takes the form of:

$$Q_{rad} = K^+ - K^- + L^+ - L^- \quad (2.5.1)$$

The behaviour of electromagnetic radiation and its interaction with matter is dependent on the frequency of the EM radiation. Lower frequencies have longer wavelength and higher frequencies have short wavelength, with the shorter wavelengths having a higher energy per photon. The spectrum of sun is close to that of a black body with a temperature of 5800K[14]. While the sun emits EM radiation across almost the entire electromagnetic spectrum. The bands of significant radiation power are between 100 nm to about 1 mm. These bands are ultraviolet, visible light and infrared. The focus in this report is on the infrared also called long-wave radiation and visible light, also called short-wave radiation. The atmosphere scatters and absorbs the incident energy from the sun. This scattering by gaseous molecules that are smaller than the wavelength is called Rayleigh scattering. The molecules responsible for the scattering in the atmosphere are: O_2 , O_3 , H_2O , CO_2 . Especially O_2 , H_2O change the solar spectrum at the earth's surface. The amount of radiation scattered by this process will vary a lot depending on the location, weather and time of year. This makes it difficult to find a relationship that accurately describes radiation heat transfer for every possible point in time.

Infrared

Infrared radiation is most commonly divided in sub-regions near-infrared (0.75-1.4 μm), short-wavelength infrared(1.4-3 μm), mid-wavelength infrared(3-8 μm), long-wavelength infrared(8-15 μm and far infrared (15-1000 μm)[15]. Infrared radiation interacts with the dipoles present in single molecules which cause the atoms to vibrate. Consequence of this that infrared radiation is absorbed by a wide range of substances causing them to increase in temperature. This process runs in reverse and causes bulk substances to radiation in the infrared spontaneously known as thermal radiation. Due to the relative longer wavelength this is more commonly described as longwave radiation.

Visible light

EM radiation with a wavelength between 400 nm and 700 nm are visible to the human eye [15]. It is also the strongest output range of the sun's total irradiance spectrum and the term shortwave radiation is used to describe this spectrum.

Ultraviolet

The spectrum of ultraviolet (UV) is from 10 nm to 400 nm and divided in 3 sections ultraviolet A (400-315) , ultraviolet B(315-280) and ultraviolet C (280-100) following the ISO standard ISO-21348[15] While ultraviolet is present in sunlight it only constitutes for about 10% of the total electromagnetic radiation output produced by the sun.

2.5.1 Solar heat exchange

The sun is considered to produce a constant amount of energy. The rays of the sun are considered parallel as they reach the edge of the Earth's atmosphere. This imaginary surface, perpendicular to the sun's rays receives an average radiation intensity equal to the solar constant (I_{solar}). The word constant is a bit misleading because the earth's orbit changes 7% during the year. Therefore the average value is taken and the solar constant equals to 1367 W m^{-2} . The value of I_{solar} is constant everywhere on the earth's surface however not all points are perpendicular to the sun's rays. A more useful quantity is the solar irradiance incident on a surface perpendicular to surface horizontal plane. The absolute maximum on such a surface is calculated with equation 2.5.2 with the solar zenith angle θ_z in the case of no scattering or absorption in the atmosphere.

$$I_{solar} = \cos \theta_z \quad (2.5.2)$$

At many meteorological stations the incoming solar radiation is measured. With such measurements available the net radiation can be directly estimated. In the case where such measurements are not available, observations of the cloud coverage N_{Cloud} and the solar elevation angle $\theta_{elevation}$ are used to estimate the incoming solar radiation.

2.5.2 Short wave radiation

The incoming solar radiation at the ground level under clear skies conditions depends to a certain extent on the solar elevation angle. A simple equation used to estimate the incoming solar radiation is shown in equation 2.5.3 with the coefficients a_1 and a_2 . These coefficients are called the turbidity coefficients and describe average atmospheric attenuation by water vapour and dust particles for a specific location.

$$K_0^+ = a_1 \sin \phi + a_2 \quad (2.5.3)$$

Research from Holtslag and Ulden (1982) found turbidity coefficients for De Bilt in the Netherlands. With values for the coefficient a_1 and a_2 respectively 1041 W m^{-2} and -69 W m^{-2} . The correlation showed an rms error of 40 W m^{-2} which is 9.5% of the observed average. It should be noted that these values are highly dependent on the location. The formation of clouds can have a significant influence on the received short wave radiation. This is most often taken into account with the total cloud fraction N_{clouds} . In meteorology an Okta is the unit of measurement to describe the cloud coverage. From clear skies at an Okta of zero and completely cloudy at an Okta of 8. An Okta of four means that sky is covered with clouds for half the visible area. An estimation of the incoming shortwave radiation used by Bruin and Wessels is shown in equation 2.5.4.

$$K^+ = 1353(0.60 + 0.22 \sin \phi) \sin \phi (1 - 0.7N_{clouds}^2) \quad (2.5.4)$$

The outgoing short wave radiation is dependent on the reflection of the surface also known as albedo α . To obtain the net short wave radiation on a surface equation 2.5.5 is used.

$$K^- = K^+(1 - \alpha) \quad (2.5.5)$$

The albedo of water is fairly constant for elevation angles of 40° , but as the angle decreases the albedo increases dramatically. Resulting in an albedo of approximately 0.5 at an elevation angle of 10° . Ice has a much higher albedo compared to water and is thus better at reflecting the incoming solar radiation. However calculating the albedo of ice is a highly complex subject. A study from

Perovich shows that the optical properties as the albedo, transmittance and extinction coefficient are related to the physical state of the ice. Therefore the albedo of both material is often taken to be constant at 6% for open ocean water and 50 % for ice. While the albedo of a material gives an easy to use estimate of the reflected solar radiation. In reality the solar radiation penetrates the layer of ice and water and is reflected throughout the material. The extinction of solar radiation is highly dependent on the wavelength, structure of the ice and on the sky conditions. This makes modelling complex and straightforward relations are poorly defined. A study from Perovich (1996) on the optical properties of sea-ice showed that formation of air bubbles resulted in larger albedo and larger extinction coefficients. The radiative transfer models for ice range in complexity, from a relatively simple exponential decay law to a numerical solution of the radiance field in the ice. The simplest ice radiative transfer model is exponential decay relationship 2.5.6. This formulation is computationally simple however it assumes that the medium is infinitely thick and therefore represents thin ice poorly.

$$F(z, \lambda) = (1 - \alpha_\lambda) F_0(\lambda) e^{-\kappa_\lambda z} \quad (2.5.6)$$

2.5.3 Long wave radiation

The general case of long wave radiation heat transfer between grey surfaces is well described in a number of textbooks. The various methods all make the same assumptions, which are summarised as follows:

- Radiation properties are independent of wavelength.
- The surface is diffuse or specular diffuse.
- The surface temperature is uniform.
- The incident energy over the surface is uniform.
- The surfaces of the enclosure do not specularly reflect radiation.

Utilising these basic assumptions the net heat transfer between a typical surface i is defined by equation 2.5.7. Where \widehat{F}_{ij} is the view factor between the bodies. The emissivity ε is defined as the ratio of the radiant emissivity of heat of a specific object or surface to that of a black body. Emissivity is a dimensionless quantity given in the range of 0 to 1.

$$Q_i = \sum_{j=1}^N \varepsilon_i \varepsilon_j A_i \widehat{F}_{ij} \sigma (T_j^4 - T_i^4) \quad (2.5.7)$$

The special case where a small object(surface) is surrounded by a large enclosure (surface 2). With these condition the ratio of A_1/A_2 approaches zero and the view factor reaches unity. Reducing equation 2.5.7 to equation 2.5.8. The result is not dependent on the surface properties of the large enclosure because almost none of the radiation emitted is reflected back on the small surface. The large enclosure can thus be seen as a blackbody absorber. This equation applies for a flat plat radiating to the open sky without interference.

$$Q_1 = \varepsilon_1 A_1 \sigma (T_2^4 - T_1^4) \quad (2.5.8)$$

The earth's surface losses heat by emitting long-wave radiation as a grey body shown in equation 2.5.9 where ε is the emissivity of the surface and T_s the surface temperature and σ the Stefan Boltzmann's constant.

$$L^- = \varepsilon\sigma T_s^4 \quad (2.5.9)$$

The emissivity of water is approximately 0.97 and taken to be 1 in the calculations for now. The maximum heat flux loss at the ice melting point is 313 W m^{-2} . The most difficult heat flux to estimate is the downward long-wave radiations as it depends on the temperature distribution throughout the entire atmosphere. It depends on the cloudiness and humidity and varies greatly, in winter it is typically in the range of 200 W m^{-2} - 300 W m^{-2} . Due to its magnitude, a small error can lead to large discrepancies in predicting the ice-growth. Many different parameterizations have been suggested that combine the clear sky conditions with one for cloudy conditions linked to the atmospheric conditions at the surface [16] [17]. These atmospheric conditions are the temperature, fractional cloud coverage and relative humidity. This allows it to be used based on forecast data from coming weather sites. The relation is shown in equation 2.5.10 where T_a is the ambient temperature in Celsius, P the water vapour pressure in hPa and the cloud coverage from 0 to 1 as N_{clouds} .

$$L^+ = \sigma T_a^4 (0.746 + 0.0066P)(1 + 0.26N_{clouds}) \quad (2.5.10)$$

The water vapour pressure is thus unknown but only depends on the the temperature of the ambient air and can thus be calculated by using one of the many approximations available in literature. To better show the effect of each of the parameters in the net long wave radiation equation 2.5.10 is plotted with the ambient air temperature on the x-axis and the net long wave radiation on the y-axis. Three pairs of lines show the situation for overcast ($n=1$), partly cloudy ($n=0.5$) and clear skies ($n=0$). The case of relative humidity of 100% is shown in the top of the pair and the bottom line is with a relative humidity of 80%. The figure clearly shows that the net output is highly dependent on the cloud fraction, to a lesser extent on the ambient temperature and probably in the margin of error from a relative humidity of 60% to 100%. The upward long wave radiation in the figure is calculated based on a surface temperature of 0°C . Using the relation of 104 W m^{-2} for 1mm of ice growth per hour as shown earlier in this chapter. Radiation can cause ice growth at an rate of up to 0.7 mm per hour for an outside temperature of 0°C and clear sky conditions. It is therefore expected that radiation plays a significant role in low temperature ice growth.

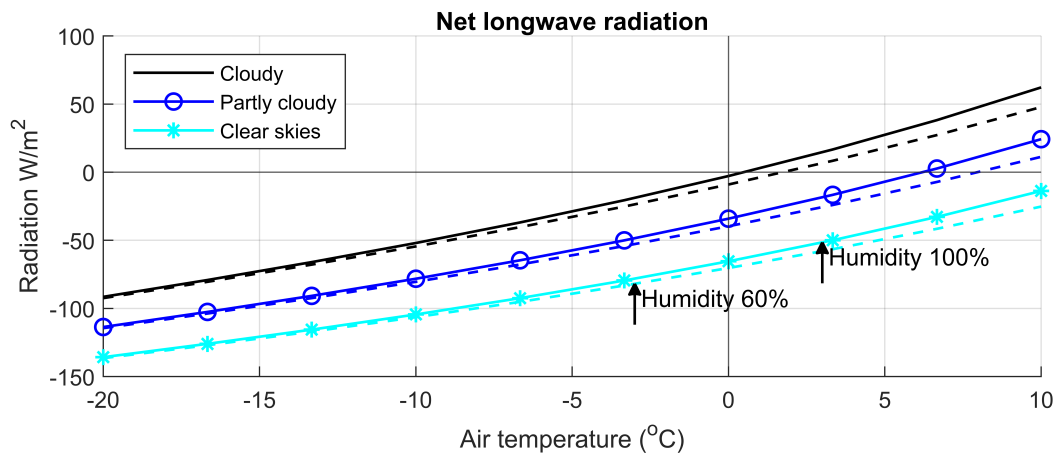


Figure 2.5: Net longwave radiation from a zero degree ice surface.

2.6 Conclusion

The different modes of heat transfer on an ice rink are conduction, convection, shortwave, and longwave radiation. Long wave radiation is the largest contributor to ice growth at low temperature conditions. This factor is largely dependent on the cloud coverage and ambient air temperature and can result in an ice growth rate of 0.7mm/h with a clear sky at an ambient temperature of 0 °C. In the case of complete overcast skies, the net long wave radiation reduces to a minimum. It is thus unlikely to see any severe ice growth during overcast conditions and most probably only if the ambient temperature is sufficiently below freezing. While the upward long wave radiation can be well estimated, the contrary holds true for downward radiation. Errors in the net long wave radiation will therefore find their source in the parametrization of downward long wave radiation. In the case of a large temperature difference between the ground surface and ambient air, convection plays a crucial role in cooling down the surface with the heat transfer coefficient ranging up to 30 W m⁻² for windy conditions. Heat loss by means of turbulent heat flow is shown to vary greatly on the atmospheric stability as well as the wind velocity, while it can temporarily increase the growth or melting of ice. Moreover, the wind velocity drops down during night time, which further decreases its ability to benefit ice growth. Driver of ice melt is the shortwave radiation from the sun, however this is only during the daytime cloud coverage and also shorter days can limit the sun's ability to melt ice. The energy transfer by means of evaporation is severely limited at air temperature below 0 °C and are expected to not play a significant role in the growth or melt of ice. In addition to this, the ambient air already has a relative high humidity during night time because of a drop in air temperature limiting its ability to transfer water. The heat transfer via conduction to the ground has a lower magnitude compared to the long-wave radiation balance and shortwave radiation, however the ground has the ability to store thermal energy for a long time and discharge this continuously throughout the day. Especially in the case of a sudden change in atmospheric conditions, this constant release of internal stored heat could prevent ice from growing. The first step in answering the question if insulation helps ice growth on ice skating rinks is done by creating small-scale ice floor setup. This experimental setup is discussed in the next chapter and allows to see the differences between insulating the asphalt layer and using a standard ice floor configuration. In the following chapter, an ice growth model is created which incorporates different modes of heat transfer and allows to see the effect of changing the ambient conditions as well as change the design of the ice rink floor. This ice growth model will be a necessary addition to the literature which primarily focuses on ice growth on open water instead of ice growth on ice skating rinks.

Chapter 3

Ground isolation experiment

3.1 Intro

An outdoor ice skating rink exists out of several different layers. The granular subbase forms the lowest layer of the structure and acts as foundation for the road profile. Size of the granular material is between 0 and 32 mm. On top of this, an intermediate layer of asphalt is placed which has an additional layer of asphalt on top with a smoother finish and is more resistant to wear. This method of building up the road is widely used because of the cheap materials used and has been tested throughout the years. Downside of this configuration of materials is that the granular subbase has a high density, thermal conductivity, and specific heat compared to, for example foamed concrete. In most use cases, insulation is not needed for the road surface, therefore limited options are available and researched. While the top and intermediate layer of asphalt also have unfavourable specifications. These layers need to be of sufficiently strong materials and have the correct properties as, for example: smooth surface, resistant riding surface and offer durability against the traffic and climate. To be able to study the effect of insulating an asphalt layer and validate the expected result, a test setup has been designed and created. This test setup has been placed at the University of Twente during the months January, February, and March of 2020. In the following sections, the setup and results of the experiment are presented.

3.2 Estimation of insulation benefit

In this section a basic estimate has been made of the heat transfer from the ground to the surface of the ice skating rink. The energy flow through the layers can be calculated with equation 3.2.1 where k_i in (W/mK) stands for the thermal conductivity of material i en L_i in (m) for the thickness of the material. The temperature gradient is denoted by ΔT in (K) resulting in the energy flow given by w/m^2 . This calculation assumes that the temperature difference is constant over time, in reality, the ground temperature would slowly decrease as the energy transfers to the surface.

$$\dot{q} = \frac{\Delta T}{L_1/k_1 + L_2/k_2} \quad (3.2.1)$$

As estimation, the commonly used values for an ice skating rink are used, corresponding to a granulated layer of 0.250m and a asphalt layer of 0.1m. Hereby, the assumption has been made that the ground temperature at a depth of 0.35m is 5.5 °C. The average soil temperature in the winter months from research in Wageningen [18]. In comparison, the layer of granulate is replaced by foamed concrete with the same thickness. By integrating the heat flux from the ground over time the total energy absorbed per unit surface area can be calculated. Using the heat of fusion

and density of ice an estimation of the ice thickness that melts over time by conduction only can be calculated as seen in equation 3.2.2. The used values for the materials are presented in table 3.1 with the corresponding ice height for a period of 8 and 24 hours.

$$h_{ice} = \frac{\dot{q}t}{\Delta H_{fus}\rho_{ice}} \quad (3.2.2)$$

Table 3.1: Height of melted ice layer for a time period of 8 and 24 hours.

Material	$k(W/mK)$	$(q)(W/m^2)$	$h_{ice}(mm), t = 8h$	$h_{ice}(mm), t = 24h$
Granulate	1.1	20	1.4	5.6
Foamed concrete	0.11	2.4	0.17	0.7

The results in the table show that insulating the asphalt layer has a significant effect on preventing the melting of ice, and thus it is beneficial to further investigate the possibility of insulating the ice skating rink. In the 24 hour scenario only by conduction from the bottom already 5.6mm of ice melt compared to only 0.7mm with the use of foamed concrete. Taking into account that for an ice skating rink with asphalt only 10-20mm is necessary to be usable, the effects are quite large. Furthermore, the relation between the soil temperature and melted ice is linear, and thus a higher soil temperature would make it even more beneficial to have insulation.

3.3 Method

To measure the effect of insulating the asphalt layer, a small scale section of the ice skating track has been built. The materials tested are Yalibims, foamed concrete, and mixed granulate. The setup with granulate materials exist out of a layer of 250mm granulate, Yalibims has a layer height of 180mm, and the last setup with foamed concrete has a thickness of 150mm all with an asphalt plate top. The dimensions of the asphalt plate are 500x500x80mm. Three temperature sensors are placed at the centre of the asphalt each with different heights.

To obtain the temperature and wind velocity near the setup a weather station is positioned close to the experimental setup. The weather station sends its data directly to a public website where that data is stored and visible for other users of the site. The weather station is shown in fig 3.1a.



(a) WS-5500 weather station next to the setup to gather temperature, wind velocity and solar intensity data.



(b) Setup of 150mm foamed concrete and 80mm top layer, surround with isolation material.

To keep the problem 1-dimensional in the vertical direction, an insulating layer has been placed around the setup. Only two plates of asphalt were available at the University therefore in the first part of the experiment the plates were placed on top of the granulate and Yalibims materials, in the second part the plate with Yalibims was moved and positioned on top of the foamed concrete setup. During the experiment, the focus of Winterswijk was primarily set on the difference between foamed concrete and mixed granulate. This was due to the fact that foamed concrete was the only

viable option for the case of Winterswijk. Due to this change in focus, primarily the differences between mixed granulate and foamed concrete are discussed.

The setup makes use of a micro controller which is connected to DS18B20 temperature sensors which have an accuracy of $0.5\pm$ between the temperature interval -10°C to 85°C [19]. This micro controller gathers the temperature data of the sensors and sends these by WiFi to a website. This website receives this information and stores it into the database.

3.4 Results

Temperature data for the setup with Yalibims and Granulate are collected from February 8 till February 17. After which the Yalibims setup has been switched to foamed concrete till 23 February. Figure 3.2 shows the temperature 2 cm below the surface for both foamed concrete and granulate for the time period 18 till 23 of February. The dotted line shows the outside temperature measured by the weather station. The graph shows that the temperature measurements for the setup with and without isolation are almost equal to each other. After the sunset a difference in temperature starts to get visible which increases with time. The temperature of the asphalt with isolation from foamed concrete shows a temperature difference of up to 2.5°C compared to the asphalt without insulation.

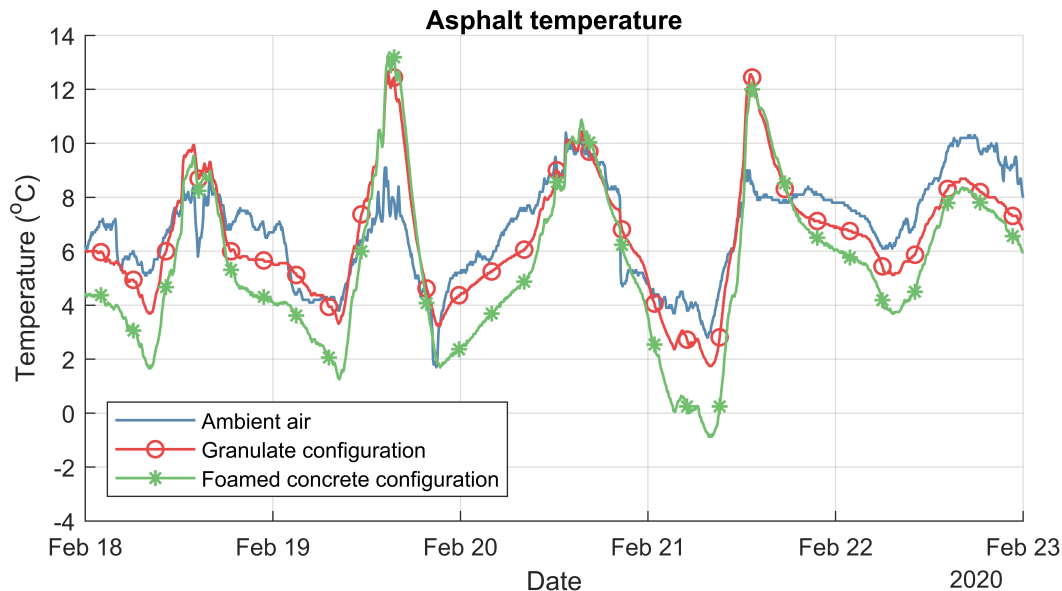


Figure 3.2: Temperature profile of the top layer of asphalt for both foamed concrete and granulate compared to outside temperature.

In figure 3.3 the temperature profile of both setups are enlarged for the night of February 20 till February 21. Temperature of both asphalt layers start to descend after the sun has set and start rising again after sunrise. The foamed concrete asphalt layer shows a sharper descend and obtains a minimum temperature below freezing, while the granulate asphalt layer cools down to just below 2°C . Both layers of ice asphalt are cooled below the ambient temperature measured by the weather station.

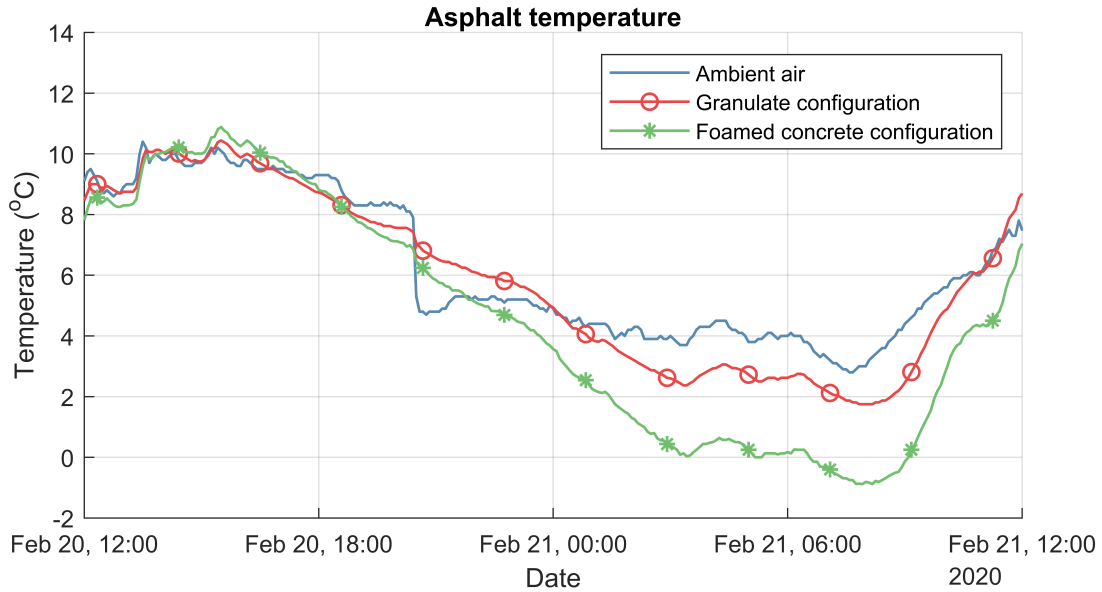


Figure 3.3: Temperature profile of foamed concrete and granulate in the night of 20 February.

3.5 Discussion

Sensors used are the DS18B20 which have an accuracy of 0.5°C in the range of -10°C to 85°C . According to the error curve, the 3-sigma error at zero degrees Celsius is $+0.15^{\circ}\text{C}$ and -0.45°C [19]. The measured temperature difference in the temperature profile plot are larger than this therefore it can be concluded that there is a significant difference between both setups even with maximum error. The temperature readings of the sensors agreed with each other within a margin of 0.5°C during a test with water at room temperature. The heat loss to the environment is dependent on the temperature of the surface. As the body radiates less heat to the surroundings at lower temperatures. Therefore, the difference in temperature can be considered as the minimum difference between insulating and not insulating. While there is no data available about the water content of the ground, literature showed that there is a significant effect related to water content and thermal conductivity. Foamed concrete is not permeable to water and therefore the thermal conductivity does not change. In the case that the setup has wet granulate material and thus a higher thermal conductivity. Redoing the experiment with material that has a lower water content would see less of a difference in temperature due to the granulate material insulating better dry.

3.6 Conclusion

Results of the test setup show a clear difference in temperature between the asphalt layer with granulate material and the asphalt layer with foamed concrete. The temperature near the surface of the asphalt descends during the night up until 1.5°C - 2.5°C lower compared to using the asphalt with granulate material. Due to the lack of strong winter temperatures, there is not data available on outside temperatures below freezing. It is expected that with lower ambient temperatures the difference between the top surface layer temperature with insulated asphalt and asphalt would increase. Insulating the layer of asphalt helps to reduce the asphalt layer temperature. Calculations show that during a period of 24 hours the melting of 4.9 mm is avoided by using foamed concrete to insulate the asphalt. Therefore, it can be concluded that a more robust ice layer is created in the case of using foamed concrete compared to granulate material as base layer. In the next chapter the ice growth model is discussed and verified based on the temperature data from the experimental setup. This allows for comparison of different different ice floor configurations.

Chapter 4

Modelling ice growth on an ice skating rink

In this chapter the ice growth model is described. With this model, the temperature profile of the ground is fully simulated as well as the layer of water/ice. This allows the user to see the actual impact of the thermal conductivity of the bottom layer. The ice growth model should be able to completely model the growth of ice based on only the meteorological variables. These being the ambient air temperature, wind speed, relative humidity and cloud coverage. This allows it to be used to predict if it is possible to create a certain layer of ice during the night. In the next chapter, the model will be tested on an experimental setup placed at the University of Twente. Because the model makes use of meteorological variables, the boundary conditions will be irregular, which makes having an analytical solution nearly impossible. Therefore, it has been chosen to solve the problem of ice growth with a numerical scheme built in Matlab. The model makes use of finite volumes of materials in which the temperature and properties are equal. The problem of ice growth is taken to be one-dimensional as the energy source is strictly from the top surface. These assumptions are listed below and will be further discussed in this chapter.

To set up a mathematical model of ice growth, a clear picture of the underlying assumptions is needed. Since the model concerns the phase change process of water, it will involve different physical properties for each phase. For simplification, it is assumed that the density is constant in both phases, which is a necessary but slightly inaccurate assumption. The phase change material has a constant melting temperature and latent heat. Furthermore, no supercooling, gravitational, or chemical effects are incorporated. The surface between each phase is assumed to be separated by a sharp, planar interface with zero thickness and no surface tension. Furthermore, it is assumed that the heat transfer is one-dimensional in the vertical direction.

The first section of this chapter discusses the heat transfer of the ground and the finite element method used. The next part discusses the relationships used in the model to estimate the other modes of heat transfer.

4.1 Finite volume method

The ground is divided into volumes each with constant properties seen in figure 4.1. For the sake of simplicity, only several volumes are shown in figure 4.1. The height of a ground layer is denoted with Δx . First, the general case is considered where Δx is constant for all layers and no phase transition. Writing the energy balance for block 2 shows equation 4.1.1. Denoting the density of the material with ρ the surface area with A , specific heat with C_p and the thermal conductivity with k .

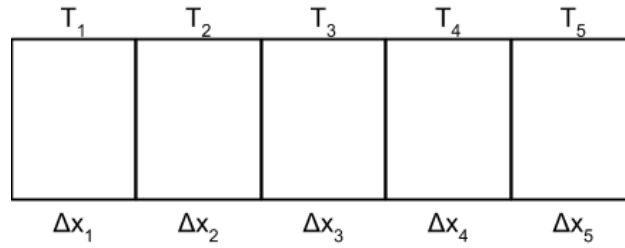


Figure 4.1: Finite volume method schematic.

$$\Delta x \rho A C_p \frac{dT_2}{dt} = kA \frac{(T_1 - T_2)}{\Delta x} + kA \frac{(T_3 - T_2)}{\Delta x} \quad (4.1.1)$$

Rewriting the equation to get all material properties on the right side gives equation 4.1.2. The equation can be further simplified by substituting the thermal diffusivity ($\alpha = \frac{k}{\rho C_p}$). Discretizing the equation results in the temperature at point t and the temperature at point $t + \Delta t$. With constant timestamp Δt this is written as iteration count i and $i + 1$.

$$\frac{dT_2}{dt} = \frac{k}{\rho C_p} \frac{(T_1 - T_2)}{\Delta x^2} + \frac{k}{\rho C_p} \frac{(T_3 - T_2)}{\Delta x^2} \quad (4.1.2)$$

$$\frac{T_2^{i+1} - T_2}{\Delta t} = \frac{k}{\rho C_p} \frac{(T_1 - T_2)}{\Delta x^2} + \frac{k}{\rho C_p} \frac{(T_3 - T_2)}{\Delta x^2} \quad (4.1.3)$$

Further rewriting the equation to obtain the new temperature at iteration ($i + 1$) results in equation 4.1.4. Take note that all other temperatures are from the previous iteration count (i). For the sake of clarity, the suffix is left out and only ($i + 1$) is shown.

$$T_2^{i+1} = T_2 + \frac{k\Delta t}{\rho C_p \Delta x^2} (T_1 - 2T_2 + T_3) \quad (4.1.4)$$

The parameter group seen in equation 4.1.4 is commonly known as the dimensionless Fourier number. It characterises the transient heat conduction and is the ratio of conductive transport to the thermal storage rate.

$$Fo = \frac{k\Delta t}{\rho C_p \Delta x^2} \quad (4.1.5)$$

This way of solving the transient heat conduction equation is known as an explicit method. Explicit methods calculate the state of the system at a later time from the current state of the system where as an implicit methods find the solution by solving an equation involving the current state of the system and the later one. The major drawback of the explicit method is that it is much harder to implement. While the explicit method is easier it has the downside of numerical instability.

4.1.1 Numerical instability

When using the explicit method care should be taken to avoid numerical instability. This happens when the timestamp Δt is too large after which the model disobeys the second law of thermodynamics. This instability is often hard to describe in non-linear or complex systems. In the case of the heat conduction discussed above the stability condition follows the form seen in 4.1.6. This can be visually represented as seen in figure 4.2, in the first figure the temperature of block two is

larger than the surrounding blocks. In the next iteration the subtracted energy is so large that the temperature is below the surrounding blocks and thus voiding the second law of thermodynamics. In this case the solution is stable if $Fo \leq 0.5$. The Fourier number is dependent on the material properties, time step and spatial step. The material can of course not be changed in the model. Reducing the spatial step results in a quadratic decrease in time step to satisfy the stability criterion. In the model care should be taken to satisfy the strictest stability criterion. In this example the stability criterion is based on conduction from the blocks surrounding it. However it could be the case that the block at the boundaries has a stricter criterion. In the model a check is placed to detect numerical instability and warns the user.

$$1 - 2Fo \geq 0 \quad (4.1.6)$$

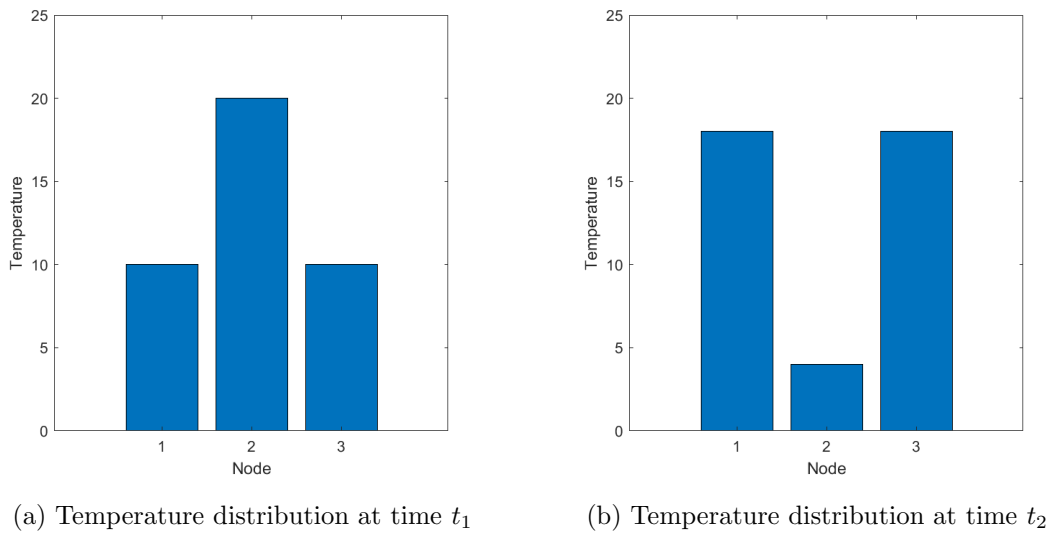


Figure 4.2: Visual representation of instability criteria, energy flows from lower to higher temperature.

4.1.2 Interface resistance

In the ideal case the material has uniform properties, in this section an addition is made to the model to be able to calculate different set of materials. In the case of a boundary between two different materials the interface resistance is calculated following equation 4.1.7 where $R_{i,j}$ denotes the interface between block i and j . With the interface resistance the energy flow via conduction is calculated with the formula as seen in equation 4.1.8. This is to be done at both interfaces, and thus the bottom and top interface. Only the boundary blocks have a specified boundary conditions and thus only have one conduction interface.

$$R_{i,j} = \frac{\Delta x_i}{2k_i A} + \frac{\Delta x_j}{2k_j A} \quad (4.1.7)$$

$$Q_{i,j} = \frac{T_j - T_i}{R_{i,j}} \quad (4.1.8)$$

4.1.3 Temperature and enthalpy

The specific enthalpy of a volume is defined by its temperature T shown in equation 4.1.9 where C_p is the specific heat in $\text{J kg}^{-1} \text{K}$ and T_{Ref} the reference temperature which is set to be -30°C in the model. While the specific heat of a material depends on the temperature, a fixed value is used to not further complicate the calculations and the difference is often negligible when working with small temperature differences.

$$h = C_p(T - T_{Ref}) \quad (4.1.9)$$

All materials without a phase change follow this relation, however water behaves differently and the specific enthalpy depends on temperature and ice fraction x . The specific enthalpy before the phase change temperature T_{Fus} follows the temperature linearly after which the enthalpy increase with the ice fraction x . Only after the phase change is completed and the ice fraction is 1 the specific enthalpy linearly increases with the temperature. The relation for calculating the temperature from the specific enthalpy is given in equation 4.1.12. The specific enthalpy at the onset of freezing h_0 is shown in equation 4.1.10 and the specific enthalpy when completely frozen is given by equation 4.1.11.

$$h_0 = C_p(T_{Fus} - T_{Ref}) \quad (4.1.10)$$

$$h_1 = C_p(T_{Fus} - T_{Ref}) + \Delta H_{Fus} \quad (4.1.11)$$

$$T = \begin{cases} T_{Ref} + \frac{h}{C_{p,ice}} & h < h_0 \\ T_{Fus} & h_0 \leq h \leq h_1 \\ T_{Fus} + \frac{h-h_1}{C_{p,water}} & h > h_1 \end{cases} \quad (4.1.12)$$

,

4.1.4 Enthalpy method

Using equation 4.1.1, which show the energy balance for a normal block via conduction. Is not valid when using water because the energy in a block is not directly proportional to the temperature increase over the entire temperature region, as shown in section 4.1.3. To overcome this non-linearity in the model the total enthalpy of the block is used and written on the left side of equation 4.1.1 and using the same steps the total enthalpy at the end of an conduction step is given by equation 4.1.13. The new enthalpy of the block allows to calculate the specific enthalpy which in turns gives the temperature from the relations shown in equation 4.1.12.

$$H_2^{i+1} = H_2^i + kA\Delta t \frac{(T_1 - T_2)}{\Delta x_1} + kA\Delta t \frac{(T_3 - T_2)}{\Delta x_3} \quad (4.1.13)$$

4.2 Turbulent energy flux

The heat transfer by turbulent movement in the model is a boundary conditions at the top surface. The energy flux is calculated from the equation described in section . The equations are presented below for sake of readability. These relations are again not linear and thus normal ways of solving the problem is not possible and thus this boundary conditions is solved at every single time step.

The calculated energy flux is added to the top block in the model and spreads from there via conduction.

$$h = 2.5U_{10} \quad T_s \leq T_a \quad (4.2.1)$$

$$h = 2.5U_{10} \left[\frac{1 + 10(T_s - T_a)}{U_{10}^2} \right]^{1/2} \quad T_s > T_a \quad (4.2.2)$$

$$Q_{convection} = h(T_a - T_s) \quad (4.2.3)$$

4.3 Longwave energy flux

As previously discussed in section 2.5.3 the outward long wave radiation is described by equation 4.3.1. The more complex part of the longwave energy flux is the incoming longwave radiation which is dependent on the ambient temperature, water vapour pressure and cloud coverage. The used empirical relation is shown in equation 4.3.2.

$$L^- = \varepsilon \sigma T_s^4 \quad (4.3.1)$$

$$L^+ = \sigma T_a^4 (0.746 + 0.0066P)(1 + 0.26N_{clouds}) \quad (4.3.2)$$

The water vapour pressure is given by the Buck equation [20]. The Buck equation gives the water vapour pressure in kPa with the temperature in °C. The empirical relation is shown in equations 4.3.3. The longwave energy flux is either subtracted or added to the topmost block of the model.

$$P = 0.61121 \exp \left(\left(18.678 - \frac{T}{234.5} \right) \left(\frac{T}{257.14 + T} \right) \right) \quad (4.3.3)$$

4.4 Shortwave energy flux

The shortwave energy flux is the radiant energy coming from the sun and the empirical relation shown in section 2.5.2 is used. The empirical relation uses the elevation angle and cloud coverage.

$$K^+ = 1353(0.60 + 0.22 \sin \phi) \sin \phi (1 - 0.7N_{clouds}^2) \quad (4.4.1)$$

The elevation angle is the angle between the sun's rays and horizontal plane measured in the vertical plane. The zenith angle is closely related to the solar elevation angle. It is the angle between the sun's rays and the vertical. Since these two angles are complementary the cosine of either of them equals the sine of the other. By using the spherical trigonometry both angle can be calculated with the relation in equation 4.4.2. A variety of angles are needed and the equation used in the model are discussed below.

$$\cos \phi_z = \sin \phi_{Ele} = \sin \phi_{Lat} \sin \phi_{Dec} + \cos \phi_{Lat} \cos \phi_{Dec} \cos \phi_{Hour} \quad (4.4.2)$$

- ϕ_z is the solar zenith angle

- ϕ_{Ele} is the solar elevation angle
- ϕ_{Lat} is the local latitude
- ϕ_{Dec} is the current declination of the Sun
- ϕ_{Hour} is the hour angle

4.4.1 Declination angle

The declination angle is the angle between equator and a line drawn from the centre of the Earth to the centre of the sun. The seasonal declination angle varies from -23.45° to 23.45° during the year. An accurate relation for the declination of the earth is given by equation 4.4.3 where N is the day of the year with January 1 as $N = 0$.

$$\phi_{Dec} = \arcsin \left[\sin(-23.44^\circ) \cdot \cos \left(\frac{360^\circ}{365.24}(N + 10) + \frac{360^\circ}{\pi} \cdot 0.0167 \sin \left(\frac{360^\circ}{365.24}(N - 2) \right) \right) \right] \quad (4.4.3)$$

4.4.2 Hour angle

The hour angle ϕ_{Hour} at a point on the earths surface is the angle through which the earth would turn to bring the meridian of the point directly under the sun. At solar noon, at the observer longitude the hour angle is 0° and the sun reaches its highest position in the sky. Time before the solar noon is expressed as negatives degrees and the time after solar noon expressed as positive degrees. The hour angle is thus the angular displacement of the sun east or west of the local meridian and measured with 15° per hour. For example the at 13:30 the hour angle is 22.5° .

4.4.3 Shortwave absorption and reflection

The model is now capable of determining the incoming solar radiation at every point during the year with the cloud coverage as only variable open for the end user. While the other heat fluxes only impact the top block of the model the solar radiation is absorbed throughout the water and ice. It is solely responsible for the interior deterioration of the ice. It can also pass through the ice and heat the underlying surface. Using the irradiance as calculated in 4.4.1 as solar energy at the top surface. Gradually reducing the intensity as it passes through the medium as it gets absorbed. This absorption is related to the absorption length λ or otherwise known as the attenuation length of a material. Equation 4.4.4 shows the radiation intensity at depth z .

$$I(z) = I_0 e^{-\lambda z} \quad (4.4.4)$$

This equation allows the model to calculate the absorbed energy for each block the solar radiation passes through. A fraction of the solar energy is directly reflected at the surface and depends on the albedo a of the ice or water. In the case that the ice layer is sufficiently thin, the solar energy also reflects at the bottom surface of the ice at the asphalt layer. The albedo of asphalt is most often much lower than that of ice which could result in the melt of ice at the bottom of the ice layer from incoming solar radiation. The albedo and absorption coefficient are fundamental optical properties of ice and can vary considerably with surface conditions and crystal structure. Also both parameters can change over time in response to the gradual melting. In this model the albedo and absorption coefficient are fixed in time.

4.5 Calculation loop

At the start of the calculation, the model reads the config file which tells the model material parameters as well as the depth of each layer. After this, each material is set to the initial conditions and the enthalpy of each block is calculated. After these steps are finished the main calculation loop is ready to run, in this loop, the boundary conditions are calculated and applied to the specific blocks as well as the conduction energy flux. After this each block has an updated enthalpy value. This is then transformed to a temperature value with the equations described in section 4.1.4. After this is all finished, the model updates time and the loop is repeated until the time passes the final time. Every few iterations of the loop all the block data is saved to an external file. This can later be used to plot temperature profiles of the ground. To save memory, it is chosen to not save the data for every single iteration step. A time step of one second for a period of one day would already have 86400 save points, which would be over the top. Because the boundary conditions do not fluctuate as much in time, it is possible to also calculate the boundary conditions every few iterations. This greatly speeds up the calculation with only little difference in outcome however this was only used during testing of the ice growth model. All figures and results from the model updated the boundary conditions for every time step.

Chapter 5

Ice growth model validation and prediction

In this chapter, the model is validated by using the temperature and environment data from the experimental setup. After verification of the model is completed, several different scenarios are calculated. This allows to make predictions about the ground temperature and ice thickness with or without insulation, as well as gain more insight in the optimal design of an ice skating floor.

5.1 Verification

Verification of the model is quite challenging because the model makes use of a variety of different parameters. This makes it hard to calibrate the model part by part because of the many iterations necessary. In addition to this, there are uncertainties about for example, the exact thermal properties of the ground layers or the accuracy of the relations used in the model. The first test of accuracy of the model is done by feeding the data of the weather station into the model and plotting the temperature profile at certain depths over time. Some of the input parameters are not known and need to be estimated.

5.1.1 Ice floor layers

A ice floor is built up by different layers each with different thermo-physical properties. In this section, the properties of each layer is discussed as well as the different configurations used in Winterswijk. The configuration without insulation exists out of the layers: soil, mixed granulate, open asphalt and closed asphalt. In the case with an insulated ice floor, the mixed granulate is replaced by foamed concrete. The asphalt normally consists of two different types of asphalt, with the bottom layer having an open structure which results in a decreased density, and the top layer having a dense graded structure to achieve an impermeable layer to water. The two different configurations used in the final model are described in table 5.2, and these two configurations are the options for Winterswijk, one configuration with insulation and one without. The other configuration in the table describes the layers of the experimental setup, in the experimental setup only a single layer of dense graded asphalt is used with a thickness of eight centimetres, compared to the two-layer variant of nine centimetres in the final model. The insulating layer is five centimetres thinner compared to the final configuration, resulting in a thickness of fifteen centimetres. The thermo-physical properties of each material are presented in table 5.1.

Table 5.1: The thermo-physical properties of each material[21].

	Cp (J kK ⁻¹)	k(W m ⁻¹ K)	ρ (kg m ⁻³)
Asphalt -D	852	1.72	2399
Asphalt-O	763	1.24	2269
Soil	1000	1.0	1700
Mixed granulate	1000	1.10	2190
Foamed concrete	875	0.19	600

Table 5.2: Configurations of the ice floor used in the experiment and model with the thickness of the layer between brackets.

Layer	Experiment	m	Normal	m	Insulation	m
1	Asphalt-D	(0.08)	Asphalt-D	(0.04)	Asphalt-D	(0.04)
2	Foamed concrete	(0.15)	Asphalt-O	(0.05)	Asphalt-O	(0.05)
3	Soil	(∞)	Mixed granulate	(0.20)	Foamed concrete	(0.20)
4			Soil	(2.00)	Soil	(2.00)

D: dense-graded, O: open-graded

5.1.2 Model input parameters

The model needs a selection of input parameters, before it can be used. These parameters are supplied by the local weather station next to the experimental setup as discussed previously in section 3.3. The weather station captures the ambient temperature, wind velocity, and relative humidity. The only fundamental parameter left for the simulation is the cloud fraction, this parameters is hard to measure with standard equipment and can vary locally. Therefore, it has been chosen to start with a fixed cloud fraction of 50% during the entire simulation.

These parameters are used in the various equations and relations described in detail in chapter 3. Allowing to calculate the energy balance at the surface. Any errors in the input parameters might get enlarged by this step, therefore care should be taken with the accuracy of the output data. The surface energy balance is then used as a boundary condition in the conduction model of the entire ground. The resulting temperature profile is the final output of the model and is what will be compared to the data of the experimental setup. While numerical stability is necessary to obtain a solution, as previously discussed.

5.1.3 Temperature profile

As the initial temperature distribution of the entire ground is unknown, it is set to 7 °C corresponding to the average temperature at a depth of 0.2m in the experimental setup. The error of this initial state will smooth out over time in the simulation. The model uses the data from March 1 until March 7 in the year 2020. The temperature data of both the model and experiment are plotted in figure 5.1. The model is shown with solid lines and the experiment with dashed lines, each colour corresponds to a certain depth. The green line is at a depth of 0.02m in the asphalt layer, the blue line is at a depth of 0.1m. The last location at a depth of 0.2m is the red line which is also placed in the foamed concrete layer.

The model starts with an initial temperature of 7 °C this is also the starting point as seen in the figure. Because the temperature of the entire layer is not completely uniform the model needs some time to adjust to the outside conditions. This is clearly seen for the temperature at 0.2m which gradually moves closer together. Larger temperature difference between the model and experiment are visible for the top sensor, especially during the maximum and minimum temperature of the day. This can be explained by the fact that during a sunny day with low cloud coverage, the

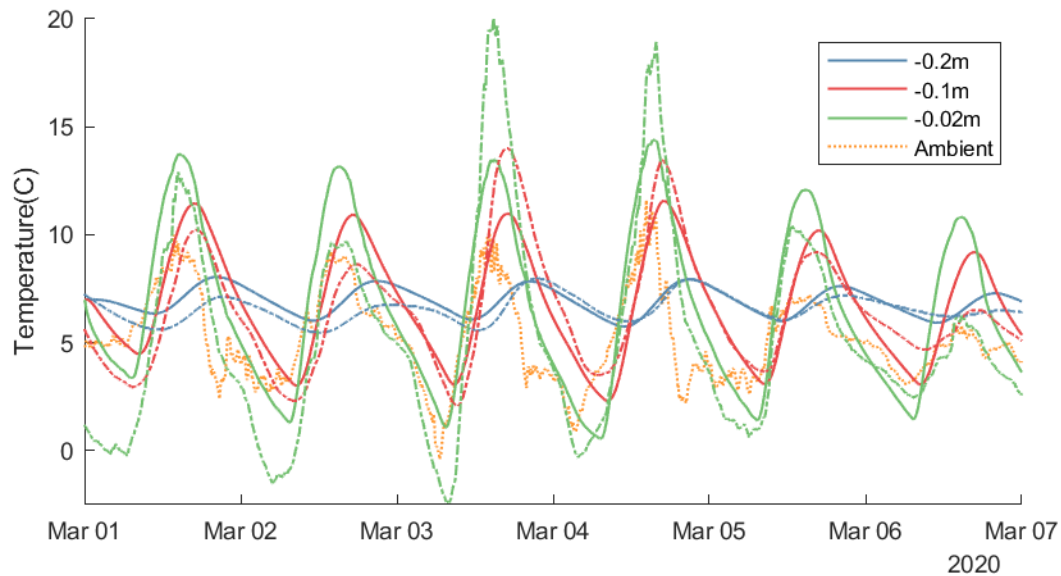


Figure 5.1: Temperature profile at certain depth over time for the insulated case. The model output is shown with solid lines and the experimental setup with dashed lines.

model underestimates the shortwave radiation reaching the surface. The same might be happening during cold nights where an open night sky allows for more radiation. While there is no exact data available about the received longwave radiation during the experiment to compare with the model. The weather station does measure the incoming shortwave radiation during the day. Data of the incoming solar radiation is compared to the model with different cloud factor settings to see if the model is accurate for determining incoming solar radiation. The resulting plot is shown in figure 5.2 with purple as the measured values by the weather station and the other lines for the shortwave intensity from clear sky ($N=0$) to completely cloudy ($n=1$).

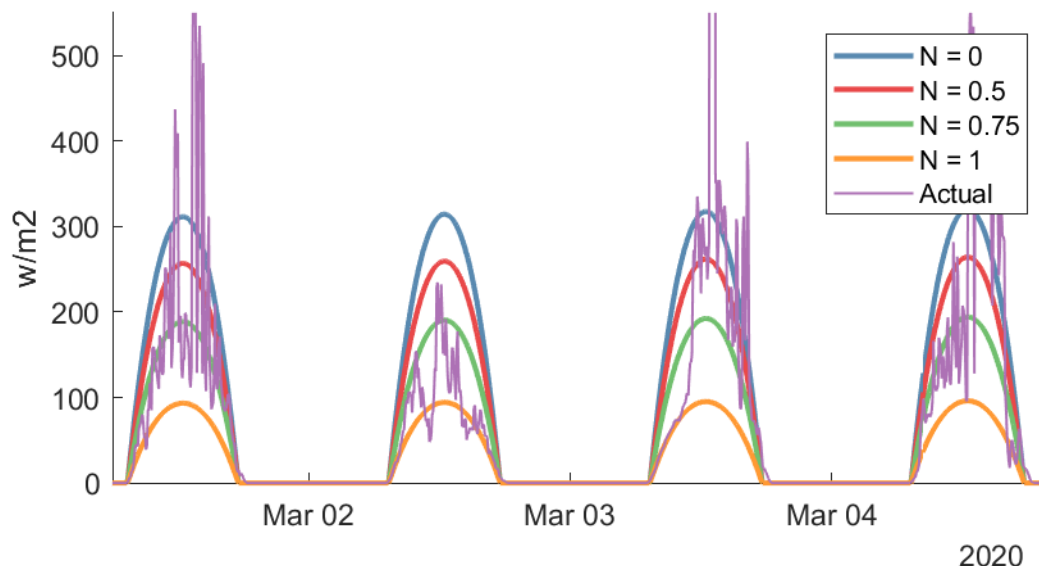


Figure 5.2: The intensity of solar radiation measured by the weather station shown by dashed line, and the model output for different cloud fractions by the solid lines.

Figure 5.2 clearly shows that the measured solar intensity does not correspond to the model with a fixed cloud coverage of 50%. It should be noted that the weather station makes use of a lux sensor

and transforms this into the thermal energy flux. However, this is not a straight forward conversion, because the intensity depends on the wavelength of the light. While there is an approximate conversion factor of 0.0079 W m^{-2} commonly used for sunlight, this does add extra error into the equation. In addition to this, the data sheet of the weather station states an accuracy of only $\pm 15\%$. This all together might explain the error between the weather station and the model. Furthermore, the sensor sometimes even gives results outside the scope of possible energy flux as seen in the figure during March 3, which shows a spike above 1000 W m^{-2} . Comparing the measured data with the expected shortwave radiation according to the KNMI for an average day in March, shows an expected max of 319 W m^{-2} from 12:00 till 13:00. In conclusion, the model makes an accurate prediction of the sunrise and sunset times, however, the lack of cloud fraction data makes it hard to get an accurate result of the actual intensity. In addition to this, there is reason to believe that the weather station data is not completely accurate making a fair comparison between the two even harder.

5.1.4 Discussion

The model shows promising results seeing that the temperature at greater depth corresponds to the model. This temperature data is less susceptible to the highly fluctuating weather conditions and the model matches up quite nicely. While the model has trouble estimating the correct shortwave radiation due to limited cloud coverage data. From March 2 to 3 the model overestimates the surface temperature because there is a day with less radiation compared to an cloud coverage of 50% and the next day the model undershoots the surface temperature because there is much more shortwave radiation present. While the model is able to calculate the temperature trend of the layers, it is not 100% accurate.

5.2 Predictions

In this section, the ice growth model is used to gain insight about the factors influencing ice growth as well as gaining insight in the optimal design of an ice skating floor. In the first instance, the difference between using a configuration with insulation and a configuration without insulation is investigated. The ice floor configurations used in the predictions are stated in table 5.2. In the simulations afterwards, only the insulated case is studied for the effect different ambient conditions have on the ice growth rate as well as the changing the asphalt layers.

5.2.1 Difference between insulated and non-insulated configuration

One of the important aspects for an ice skating association, is the ability to create an ice floor earlier during the season or earlier compared to other skating associations in the Netherlands when cold weather appears. In this scenario, the ground is still relatively warm when cold weather appears, thus it is expected that the insulation helps reduce the heat flow from the ground to the ice. The scenario used to test this starts at December 1 with the initial temperature of the complete ground set to 8°C after which the ambient temperature drops to -5°C allowing the ground to cool down by convection and thermal radiation.

5.2.2 Difference in temperature profile

The temperature data over time is plotted in figure 5.3. The isolated asphalt layer is shown in blue and the normal asphalt in red. The temperature shown are just below the surface at 0.01m , between the asphalt and foamed concrete/mixed granulate and at 0.3m at the end of the insulation.

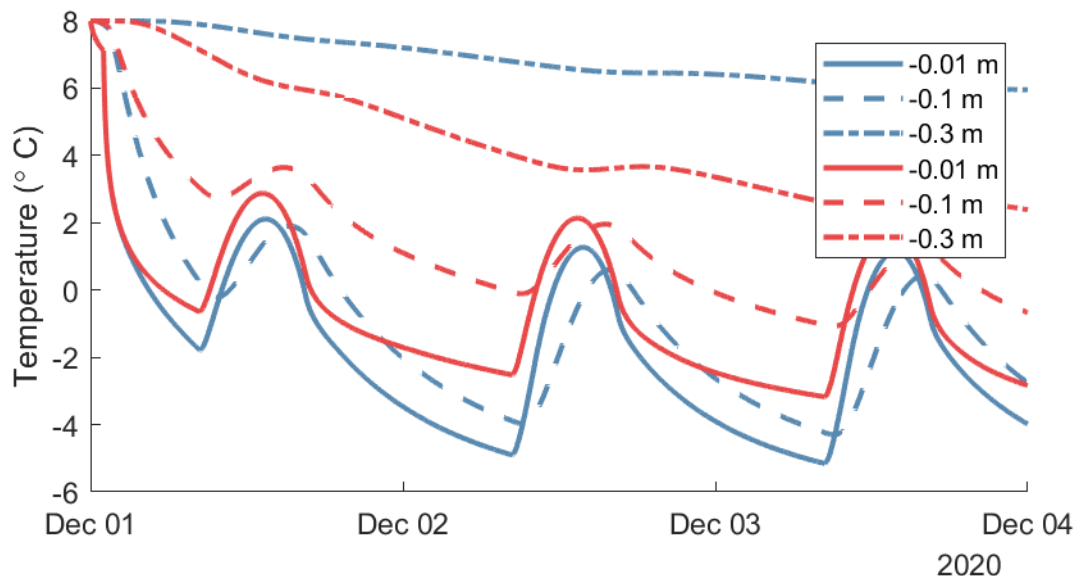


Figure 5.3: Temperature response to a sudden drop in ambient temperature from 8°C to -2°C . The blue lines correspond to the insulated setup and the red lines to the standard setup.

The surface temperatures of the insulated and non-insulated asphalt show a sharp decrease in temperature when the cold front comes. During the night, the insulated asphalt is able to reach a lower minimum temperature at the end of the night. The temperature difference in the first night is 1.1°C at 8:22 in the morning. During the second night, the temperature difference increases to 2.4°C and the insulated asphalt layer is even able to go far below the ambient temperature due to radiative cooling. At a depth of 0.3m , almost all daily fluctuations are damped as is expected. The temperature with insulation reduces to 6.0°C while the other reaches a temperature of 2.4°C . All

this energy can only go to the top surface, as the material below is even warmer. Thus preventing ice growth. This figure clearly shows the positive effects of insulation. It also shows that there is reason to believe there is a significant difference in temperature with insulation compared to without.

5.2.3 Difference in ice growth

In this scenario, the difference in ice growth is determined between the ground configuration with insulation and without. To simulate the use of an spraying cart for the creation of an ice floor. The model checks if the top two layers of water are frozen and only then adds a layer of water. The height of an layer of water is set to 0.5mm with an temperature of 10 °C. The spraying of water is only allowed between 16:00 and 06:00 as would be the case in Winterswijk. During the day, the ice skating rink is open to the public and the net energy transfer is lower compared to the night or even positive in warm conditions. For the simulated scenario, a decrease in temperature is simulated at 08:00 after which the ground has time to cool down until 16:00 and the spraying of water starts. The initial ground temperature is set to 8 °C and the ambient temperature is decreased to -3°C with the relative humidity set to 0.95 and the cloud fraction to 0.5. The simulation is run from December first at 08:00 until the fourth of December, so as to see the effect of having multiple days of cold weather. The resulting ice layer height over time is plotted in figure 5.4. The temperature profile of the ground over time is plotted in figure 5.5 for the insulated configuration and in figure 5.6 for the non-insulated ground floor configuration .

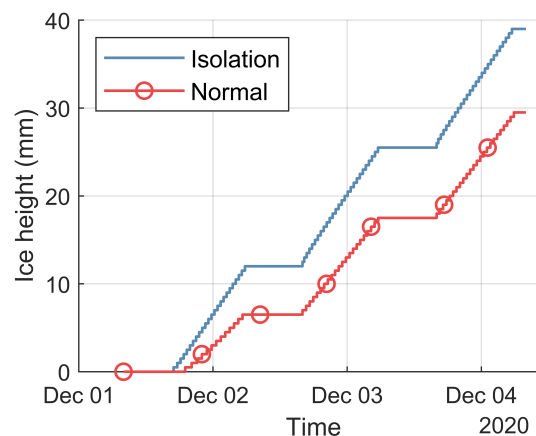


Figure 5.4: Ice layer height for insulated and non insulated ground configuration with an ambient temperature of -3°C , relative humidity of 0.95 and cloud fraction of 0.5.

The height of the ice layer over time is seen in figure 5.4 and the insulated configuration achieves an ice layer of 12mm at the end of the first night where the non-insulated achieves a thickness of only 6.5 mm. At end of the second and third night, the insulated configuration has an ice layer thickness of, respectively, 25.5mm and 39mm. The non-insulated configuration achieves an ice thickness of 17.5mm and 29.5mm during the second and third night. The total differences in the height of the ice floor between the configurations during the three nights are 5.5 mm, 8mm, and 9.5mm in favour of the insulated configuration. From the figure it is therefore possible to state that the insulated case thus achieves a thicker layer of ice during all nights, and the difference in heights increases in the following two nights.

The temperature data of both configurations are shown in figures 5.5 and 5.6 with the depth of the layer shown on y-axis and the time on the x-axis, the temperature at each point in time and space is shown with colour. The top of the asphalt layer is set to a height of zero, everything below has a negative value and the ice above has a positive value. For both configurations, there is a

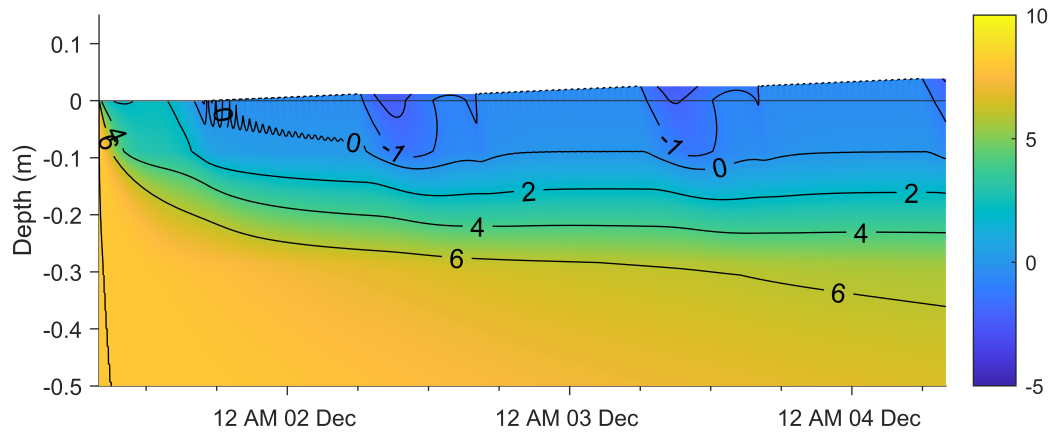


Figure 5.5: Ground temperature profile over time for the insulated configuration.

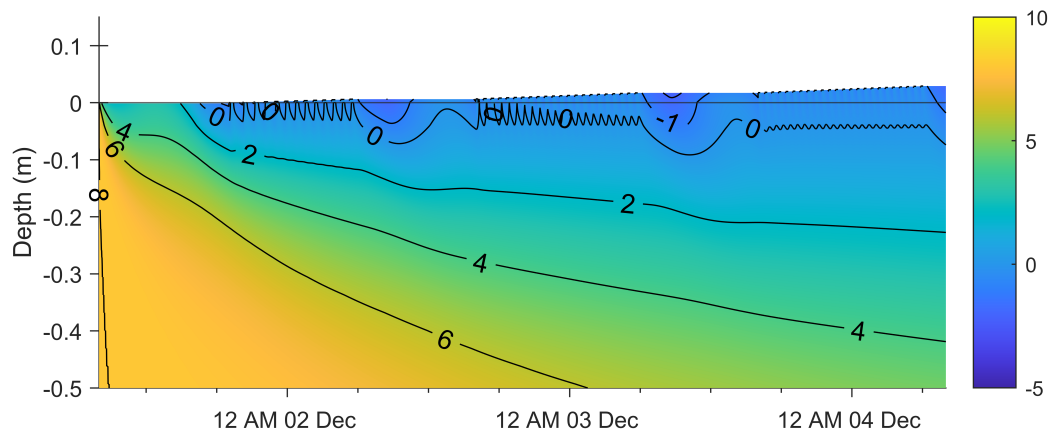


Figure 5.6: Ground temperature profile over time for the non-insulated configuration.

step decline visible in the surface temperature during the first day. While both surfaces cool down rapidly only the insulated case has achieved a surface temperature of -1°C at 16:57, surpassing the threshold for applying a layer of water. The non-insulated case achieves a surface temperature of -1°C at 19:02 on the first day, thereby reducing the available time to spray water. In the following two days, the surface temperature is able to cool down to -1°C at 16:00 and water spraying starts immediately. One of the key differences between the two temperature plots are the isotherms of 4°C and 6°C . For the insulated configuration, the isotherms stay horizontal for a longer duration, which implies that the stored heat is unable to escape to the surface during this time. For the non-insulated configuration, the isotherms move downwards implying that the stored energy is able to transfer to the surface thereby preventing ice to form. The other key difference in both temperature plots is the temperature of the asphalt during the day. With the ambient temperature set to -3°C the entire ice floor of the insulated configuration is able to cool down to a temperature of -1°C whereas with the uninsulated configuration only the top three centimetres of the asphalt is able to cool down to -1°C . In conclusion, in the case of a sudden drop in ambient temperature, replacing the mixed granulate layer with an insulating layer has a positive effect on the ice growth.

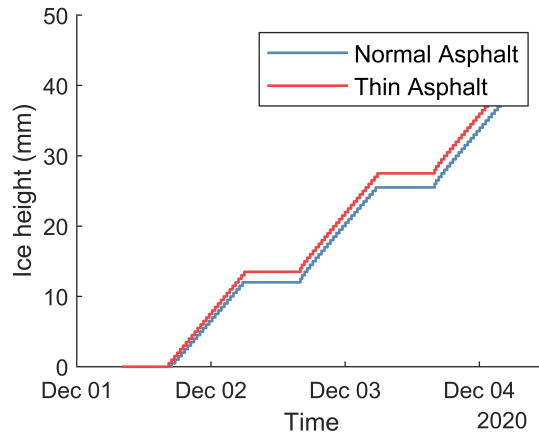


Figure 5.7: Ice layer height for insulated ground configuration with an ambient temperature of -3°C , relative humidity of 0.95 and cloud fraction of 0.5 for two asphalt configurations.

5.2.4 Effect of asphalt thickness

In this section, a configuration with a reduced asphalt thickness is tested. The proposed configuration only has a dense graded layer of asphalt, eliminating the open graded layer with a thickness of 5cm, resulting in asphalt layer of only 4 cm compared to the original 9 cm. Asphalt is a good conductor compared to other material layers and has a high density resulting in the ability to store lots of thermal energy. The ambient conditions are kept the same as before with an ambient temperature of -3°C , relative humidity of 0.95 and cloud fraction of 0.5. The corresponding ice layer height plot is shown in figure 5.7 with the ice thickness on the y-axis and the time on the x-axis. For this scenario, only the configuration with insulation is simulated.

Figure 5.7 shows the ice layer height for the thin asphalt configuration and normal asphalt configuration. With the thin asphalt configuration, an ice floor of 13.5 mm is able to form after the first night, an increase of 1.5 mm from the normal configuration. In the following two nights, the ice layer thickness is 2 mm. It can thus be concluded that the asphalt helps for the first night, however after the initial cooling the effect is not noticeable anymore. The difference of 1.5mm is also relatively minor compared to the difference seen in the uninsulated and insulated case where a difference of 5.5 mm was seen in the first night.

5.2.5 Effect of the water layer height

Use of the water spray cart allows for selection of the water layer height used during ice creation. In this section, the effect of increasing or reducing the water layer height on the speed of ice growth is investigated. The selected water layer height are 0.5mm, 2mm, and 4mm. The times when is spraying of water is allowed are kept the same from 16:00 until 6:00 in the morning and only when the top 1mm is below a temperature of -1°C . This is to ensure water is not sprayed endlessly. The insulated configuration is used with the same ambient conditions as before. The resulting ice thickness over time is plotted in figure 5.8.

The ice thickness for the 0.5 mm layer height after the first night is 12 mm as seen in figure 5.8, the ice thickness for the 2 mm layer height is 14 mm, and for the 4mm water layer height the ice thickness is 16mm. However, the last layer of water is added just before 06:00 for all three simulations. This additional layer of water at the end of the night is not completely frozen at 06:00, this is the case for 0.5 mm water layer height. During the hours after 06:00 the 2mm and 4mm freeze over completely, this additional time might be why the increased layer height performs better. However, also during the second night, the configuration with an increased water spray

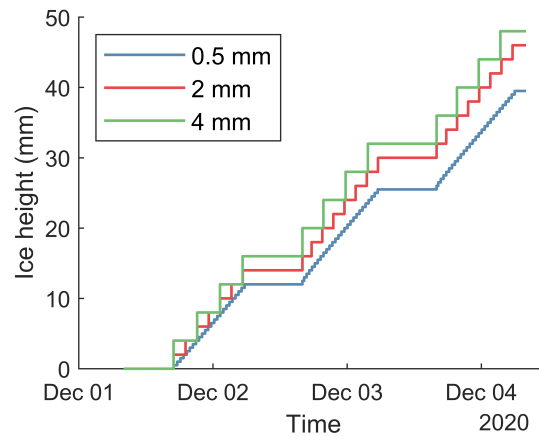


Figure 5.8: Ice layer height for insulated ground configuration with an ambient temperature of -3°C , relative humidity of 0.95 and cloud fraction of 0.5 for different water layer heights. Applying water if the top 1mm is below -0.1°C .

layer showed to be more favourable. The reason the thicker layers of water are able to grow more ice is due to the fact that the heat loss by the ice is proportional to the surface temperature of the top surface. If one compares the change of surface temperature for the three cases, the case with a thicker water layer has a longer-lasting period of "wet" surface or with a surface temperature of 0°C . This longer period with a higher temperature allows the thicker water layer to cool down more efficiently. However, if the condition of only allowing a new water layer, if the top 1 mm is below -1°C is changed to -0.1°C , the benefits of applying a thicker layer are not significant anymore.

5.3 Discussion

The three topics discussed in this chapter are whether insulating the ice track, reducing the asphalt thickness, or changing the water layer thickness affects the ice growth rate. With the results from these three different experiments, an optimal design of a natural ice skating rink is formed. First, the effect of insulating the asphalt layer is discussed. The results of the model when no water is sprayed show a difference in minimum temperature in favour of the insulated configuration as was also seen in the experimental setup. When water is sprayed during the night, the insulated configuration allows for more ice growth, however, the model assumes that the entire ground has an initial temperature above ambient conditions. If this initial temperature is reduced the difference between the two configurations would decrease as there would also be less stored energy in the ground, however for the simulated case with these ambient conditions. The results show that there is a positive effect on the rate of ice growth when insulating the asphalt layer.

A limitation of the ice growth model is the assumption of equal density of water and ice. Due to this assumption, the estimated ice thickness is underestimated in the model as the density of water is used for both phases. Another limitation to this assumption is that there are no buoyancy forces simulated in the model, which could increase the heat transfer in the top water layer by the movement of water. Due to the thin layers of water involved, it is expected that the increase in heat transfer is limited. However, additional research is needed on this aspect.

5.4 Conclusion

The model is able to calculate the temperature profile of the ground with reasonable accuracy. From the verification followed that the cloud coverage is an important factor for estimating the shortwave and longwave radiation. In the case of overestimating cloud coverage, shortwave radiation will be lower in reality. Where as during the night, overestimating the cloud coverage results in more downward longwave radiation. In the scenario which compares the performance of foamed concrete with mixed granulate when a cold front approaches. The foamed concrete setup performs significantly better, approaching a lower minimum temperature which in turn would allow more ice to form.

The model results provide the distribution of ice and ground temperature, as well as the ice layer thickness and the convective, radiative and conductive heat fluxes. The influence of atmospheric conditions, design of the ice rink floor, and spray water thickness on the rate of ice growth have been examined. The ice growth rate increases when air temperature decreases, the cloud cover decreases, and the wind speed increases. An ice floor design with an insulation layer beneath the asphalt has been shown to provide a higher rate of ice growth, compared to a standard configuration with mixed granulate beneath the asphalt. Reducing the asphalt thickness for configuration with insulated showed to be beneficial for the growth rate. However, the minimum asphalt thickness is limited by the required necessary strength to provide a protective layer.

Results from the ice growth model showed that increasing the water spray thickness could provide an increase in ice growth rate if the top surface temperature is allowed to drop below freezing point. However, if the water spraying cart applies a new layer just before the layer is fully frozen, the surface temperature is unable to drop in temperature and no significant differences in ice growth rates are visible. This result shows the importance of keeping the ice surface "wet" throughout the ice growth process.

Chapter 6

Building ice by spraying layers of water

The ice skating rink in Winterswijk wants to use a different approach to creating a layer of ice. Normally, an ice skating rink is filled with water until there is an even layer of a few centimetres across the entire track. Downside of the standard approach is the increased volume of water that needs to be frozen and the inability to change the thickness during freezing. The increased volume of water is caused by the slope present in the track, the middle of the track is every slightly higher to drain rain water during the year. Because many smaller layers are used during the ice growth process, it is important that each layer is evenly distributed across the surface to create a uniform and flat ice layer. While there are other ice skating rinks in the Netherlands that spray water on the track, most use more crude methods as for example, a slurry tanker behind a tractor. The ice skating association of Winterswijk (WIJV) wants to improve and refine this method by building three custom vehicles to distribute the water, two vehicles will be used to spray the 400m track, and the other will be used for the rectangular thousand meter squared ice rink. One of the aspects the other ice associations in the Netherlands agreed about is that its best to have as small as possible layers of water. This chapter will focus on the different types of nozzle, droplet dynamics, and distribution of water. Additional attention is directed to the distribution of water in the turn of the 400m track, leading to an alternative placement of nozzles. The results of the research were used in the production of the water spray carts.

6.1 Basic nozzle dynamics

This section describes the main principles of a water spray nozzle. For Winterswijk, even distribution of a layer of water is most important. However experience from the ice skating association in the Lier showed that stopping the flow of water during the night resulted in the nozzle freezing shut. Methods to prevent this are either using a nozzle with a very wide orifice or continuously flowing water through the nozzle to prevent freezing. The two different types of nozzles that could be used for a spray cart are divided into two types the cone nozzle and the flat jet nozzle.

6.1.1 Cone nozzle

The full cone pattern, which is usually created by giving a rotational speed to the fluid flowing through the nozzle. This rotational speed gives the spray the shape of a full cone. The angle of the cone is a function of both exit speed and the design of the nozzle. In practice, it can vary from 15° to 120° . A variation of the cone nozzle is the spiral full cone nozzle. A spiral full cone makes use of a wide nozzle orifice and the water stream is deflected again through the spiral to create the desired pattern. Disadvantage is that the spray is not evenly distributed, however, due to the wide orifice, plugging of the nozzle is nearly impossible. This type of nozzle is therefore most often used in critical systems, e.g., fire fighting systems. A variation to the cone nozzle is the hollow cone spray pattern where the liquid droplets are concentrated on the outer surface of conical shape volume.

6.1.2 Flat jet

In a flat jet nozzle, the liquid droplets are sprayed in a flat line. The determining parameters for the spray pattern are the orifice cross section and the orifice edge profile, the orifice cross section is smaller compared to the spiral full cone. In the case of a spoon flat fan, the liquid flows through a round orifice and then impacts and deflects on the surface. One of the major advantages of the flat jet nozzle is the even distribution across the spray surface.

6.1.3 Recommendation Winterswijk

One of the most important aspects for Winterswijk is evenly distributing a layer of water across the surface, therefore the flat jet nozzles are to be used in the spray carts. To prevent freezing of the nozzle, a small stream of water can be pumped through the nozzle at all times. This, however, has the downside of having to constantly move the spray cart to prevent water dripping in the same location and degrading the ice quality or even melting of the ice. The selected nozzles for the ice hockey rink are the MC3E flat spray nozzles from EUspray [22], for the spray carts on the 400m track, two sets of nozzles are purchased to extend flexibility in the amount of water sprayed during use. With the particle trajectory model, the range of the nozzle is estimated for different pressures, this allows to get the correct spacing between the nozzles. Additional benefit of using flat jet spray nozzles is the possibility to turn the nozzle if there is too much overlap between the individual nozzles. The next section discusses the flow rate and basic dynamics of a nozzle to be able to estimate which nozzle size is needed to spray enough water on the track.

6.1.4 Nozzle flow rate

To get an estimation of nozzle flow rate, Bernoulli's law can be used, presented in equation 6.1.1. The law states that an increase in the speed of fluid occurs with a decrease in static pressure or a decrease in the fluid potential energy. This equation is only valid for isentropic flows while most nozzles are not irreversible. These effects are neglected in this estimation.

$$\frac{P}{\rho} + \frac{1}{2}\rho v^2 + \rho gh = \text{constant} \quad (6.1.1)$$

If we consider two sections in the nozzle, section A at the the nozzle entrance and section B at the outlet. The height difference is negligible and so $h_a = h_b$ and setting $P_b = 0$ so P_a is the differential pressure. With the orifice diameter being much smaller than the tube diameter, the velocity is also much smaller and we can consider the velocity at point A negligible compared to B $V_a \approx 0$. This in turn allows to rewrite the equation to obtain the velocity at the outlet.

$$V_b = \sqrt{\frac{2P_A}{\rho}} \quad (6.1.2)$$

Multiplying the velocity with the orifice area results in the volume flow rate of the nozzle at a certain pressure.

$$\dot{Q} = A \cdot \sqrt{\frac{2P_A}{\rho}} \quad (6.1.3)$$

While this is a simplification of the inner workings of a nozzle. This relation is often used by manufactures. This relation shows that the flow rate has a square root relation with pressure. This information is used later in the chapter to calculate the total flow rate at a certain pressure for the spray carts. In the following section, a model of the water droplets is made to estimate the distribution of water below the nozzle and see the effect pressure or droplet size has on the distribution.

6.2 Theory spray droplet trajectory

To get a better understanding of the distribution of water coming from a nozzle, a theoretical model of the droplet trajectory is made. This gives the ability to determine the best distance between nozzles as well as show the effect each parameter has on the water distribution. The most basic case is of no gravity and drag on the droplets, thus in a straight line from the nozzle to the ground. This is the theoretical spray coverage (TSC) of the nozzle and can be calculated by taking the initial height y_0 and spray angle α of the nozzle used in equation 6.2.1. This relation is only valid for small nozzle angles and therefore not usable. An improvement to this model is the addition of gravity, under this force the droplets will curve inwards. As an additional step in the model, air drag is also taken into account.

$$TSC = 2\tan(\alpha)y_0 \quad (6.2.1)$$

6.2.1 Influence of gravity on the droplet trajectory

The equation of motion for both x and y direction are presented in equations 6.2.2 and 6.2.3. The y direction is taken to be the vertical direction of gravity. Here, m^* is the mass of the displaced medium and m^*g the buoyant force. This can be rewritten into $1 - \frac{m^*}{m}$ in the case of water droplets suspended in air the density difference is several orders of magnitude and enough to state that the buoyancy force is negligible and thus $1 - \frac{m^*}{m} \approx 1$.

$$m \frac{d^2x}{dt^2} = 0 \quad (6.2.2)$$

$$m \frac{d^2y}{dt^2} = -(m - m^*)g \quad (6.2.3)$$

The particle exits the nozzle with a velocity (v_0) at a height above the ground (y_0) and is directed with an angle α taken from the vertical axis. For convenience, the starting position in x-direction is set to start below the nozzle and thus zero at time zero. The velocities at time zero are related to the angle at which the particles leave the nozzle as shown in equation 6.2.4.

$$V_{x,0} = V_0 \sin(\alpha) \quad (6.2.4)$$

$$V_{y,0} = -V_0 \cos(\alpha) \quad (6.2.5)$$

Integrating both equations with initial conditions results in equation 6.2.7. This relation already allows to estimate the final location of the droplet and improves on the theoretical spray coverage estimate. An additional improvement to the model is the inclusion of drag on the droplet particle which will be discussed in the following section.

$$x(t) = V_x t \quad (6.2.6)$$

$$y(t) = -\frac{1}{2}gt^2 + V_y t + y_0 \quad (6.2.7)$$

6.2.2 Drag

The general drag force equation is shown in equation 6.2.8. Here C_d is the drag coefficient, ρ the density of the medium, A the cross sectional area of the object and v the velocity. It should be noted that this equation is valid for constant velocity and in the case of acceleration the Basset force should be calculated. This force describes the lagging boundary layer with a change in velocity through a medium. To avoid further complicating the solution, this force is neglected. Because the Basset force is only important in fluids with large density and high viscosity[23], neglecting this force in the case of air therefore seems reasonable.

$$F(v) = \frac{1}{2}C_d \rho A v^2 \quad (6.2.8)$$

The drag coefficient depends on the Reynolds number in a complicated fashion. The curve-fit formula in equation 6.2.9 is restricted to the interval $0 < Re < 2 \times 10^5$. In the limit of very small Reynolds numbers ($Re < 1$) the first term dominates and thus the second and third terms can be discarded. The drag coefficient over the entire range of Re is shown in figure 6.1.

$$C_d(Re) \approx \frac{24}{Re} + \frac{6}{1 + \sqrt{Re}} + 0.4 \quad (6.2.9)$$

Using the equation for the Reynolds number for small Reynolds numbers reduces the drag coefficient to $C_d(Re) = 12\eta/\rho Rv$. With $A = \pi r^2$ as the frontal area of a sphere, the drag force is rewritten as seen in equation 6.2.10.

$$F(v) = 6\pi\eta Rv \quad (6.2.10)$$

This is also known as Stokes formula. It tells that drag for a very slow moving sphere is linearly proportional to the velocity. For example, sinking grains of sand in water or tiny dust particles floating in air. While the condition of $Re < 1$ is very restrictive and often not obtained in practice. Its appealing to use because of its simplicity and its linear dependence on velocity. The second interval of interest in figure 6.1 is from $10^3 < Re < 2 \times 10^5$ denoted by the number four. The drag

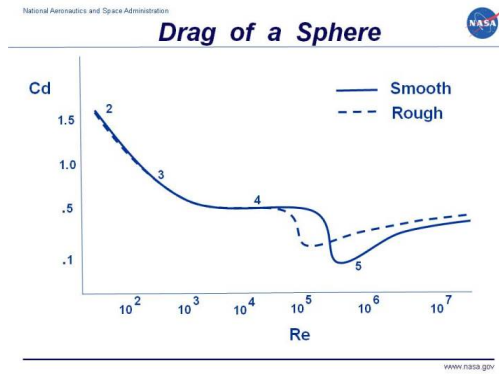


Figure 6.1: The aerodynamic drag coefficient C_d of a sphere as function of the Reynolds number Re and the surface properties [24]

coefficient is constant during this interval and the drag force reduces to equation 6.2.11. In this regime the drag on the sphere is quadratic in the velocity term and is most commonly known as "air drag".

$$F = 0.25\rho\pi r^2v^2 \quad (6.2.11)$$

The problem of the water droplet ejected from the spray nozzle can now be solved for the two regions. In practice, it is possible that a particle goes outside the domain of either linear or quadratic drag. However, water droplets are most of the time in the quadratic drag region and so we restrict our self to this region for the entire trajectory. This changes the equation of motion for both the x and y direction of the particle, adding drag results in equation 6.2.12 for the y direction and 6.2.13 for the x direction with the absolute values of velocity to always set the drag force in the opposite direction of movement. The resulting equation is solved for both x and y directions with Matlab to get the droplet trajectory. The resulting trajectory allows to estimate the max range of a nozzle or distribution of particles below a nozzle. First, the max range of a nozzle is discussed and later on the distribution and factors influencing the water distribution.

$$\frac{d^2y}{dt^2} = -g - \frac{3\pi C_d \rho_{air}}{8\rho_{sphere} r} \frac{dy}{dt} \left| \frac{dy}{dt} \right| \quad (6.2.12)$$

$$\frac{d^2x}{dt^2} = -\frac{3\pi C_d \rho_{air}}{8\rho_{sphere} r} \frac{dx}{dt} \left| \frac{dx}{dt} \right| \quad (6.2.13)$$

6.2.3 Max range of a nozzle

With the equation of motion and initial conditions known for a water droplet particle the spray range of a nozzle can be modelled. The variable parameters are the initial conditions and droplet radius. The initial velocity of the droplet is dependent on the pressure as seen in the first section of this chapter. For the selected nozzles a pressure of 1 bar is equivalent to a velocity of approximately 7.5 m/s, 2 bar is 10 m/s, and 3 Bar is 12.5 m/s. Several plots are shown in figure 6.2 to see the effect of a change in parameters to the droplet trajectory. All the water droplets start at a height of 1 meter with an initial velocity of 10 m s^{-1} or a pressure of 2 bbar at an angle of 55° and a droplet radius of 0.3 mm. Figure 6.2a shows the the particle trajectory for different angles, and it shows that with larger angles the trajectory gets more curved to the ground but also reaches further. In figure 6.2b the initial velocity of the droplets is varied, which shows a strong relation with the maximum range of a droplet. Increasing the velocity could thus make a nozzle spray wider if all

other parameters are kept the same. This is especially visible for a velocity below 7.5 m/s. In figure 6.2c the droplet size is varied which affects the drag term seen in equation 6.2.12. Smaller particles reach the ground further from the starting point, having very fine droplets could thus result in a wide spray range. Effects of the wind are left out in this model but could very well affect the trajectory especially for smaller droplets as the model shows that small droplets are most affected by drag.

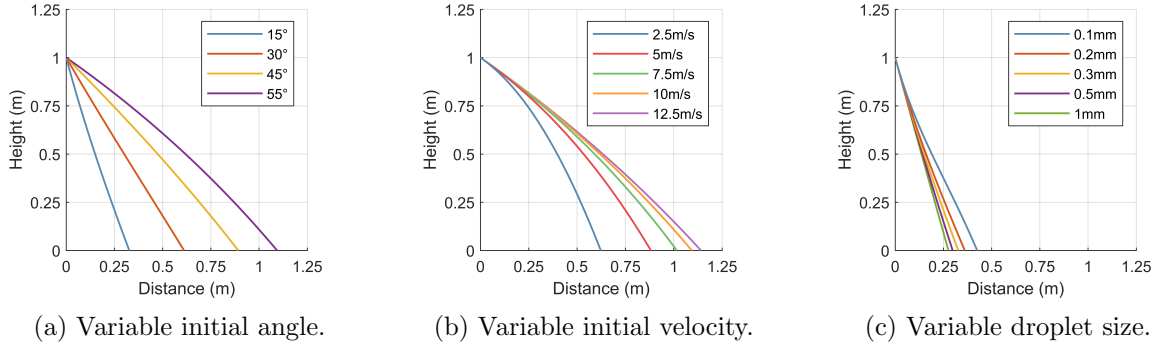


Figure 6.2: Initial angle of 55° , velocity of 10 m s^{-1} and droplet radius of 0.3 mm .

6.2.4 Water distribution of a nozzle

For the ice track it is important that each new layer of water is evenly spread out across the surface to obtain a flat surface of ice. Therefore, the distribution of water droplets needs to be determined. While there is no simple analytical solution of the distribution of droplets over the surface, a finite scheme is used to get an approximation. The model iterates over the entire spray angle of the nozzle with an angle step size of $\Delta\phi$. Every step it calculates the trajectory of a droplet particle and calculates the distance between the previous calculation, denoted by Δx . This is schematically shown in figure 6.3. Making the assumption that the water coming out of the nozzle is evenly distributed over the entire angle. It is now possible to calculate the distribution of water over the surface with equation 6.2.14. Here, the max range of the nozzle is denoted with L and max angle with α . Rewriting the step size to the ratio of the total angle/distance allows to see if more or less water is coming to that section of surface. Using a small enough $\Delta\phi$ should give an accurate estimate of the distribution of water droplets. In figure 6.4 the water distribution is given for a nozzle with a spray angle of 55° and height of 1 meter. The x-axis is the distance away from the nozzle and on the y-axis the distribution where a horizontal line at height 1 would be an even distribution over the entire spray coverage. Because a nozzle sprays in both positive and negative x-direction the plot is mirrored at $x = 0$ to get an plot of the entire spray coverage.

$$D(x) = \frac{\frac{\Delta\phi}{\alpha}}{\frac{\Delta x}{L}} \quad (6.2.14)$$

Figure 6.4a shows the water distribution in relation to the particle size. On the y-axis of the figure is the normalised distribution, a horizontal line at height one would mean a completely even distribution of water. With a particle size of 0.2 mm the distribution curve takes the shape of an V. Resulting in more water at the edges, increasing the particle size to 0.5 mm results in a more uniform distribution curve. Further increasing the particle size results in the shape of a reversed v where the outer edge get less water. In reality, a nozzle does not eject water droplets with a fixed size but over a wide range of sizes thus averaging the lines. Due to the complex nature of estimating the droplet size and time constraints this has not been studied in more detail. In figure 6.4b the distribution curve is given for different initial velocities. Its shown earlier that changing the velocity can have an effect on the range, this can be seen for the velocity of 2.5 m s^{-1} which reaches only

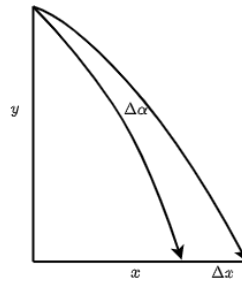
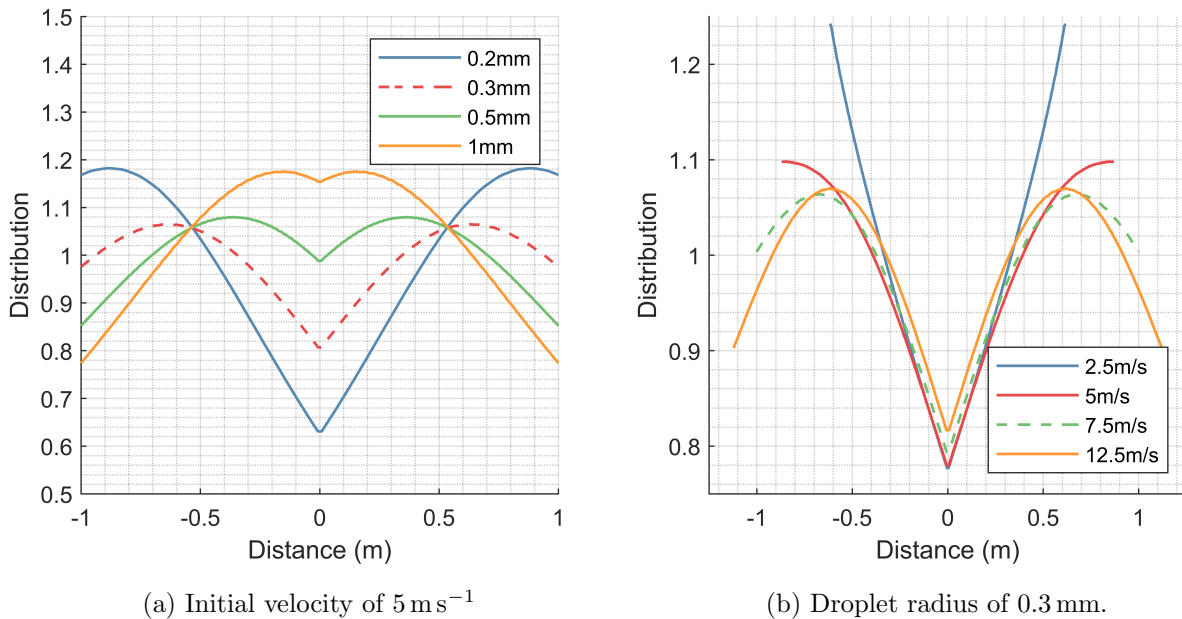


Figure 6.3: Droplet trajectory at different starting angles.

from -0.6m to 0.6m , compared to -1.1m to 1.1m for a velocity of 12.5 m s^{-1} . It should be noted that in the pressure range between 1 and 3 bar, thus between a velocity of 7.5 m s^{-1} and 12.5 m s^{-1} the range and the distribution does not change as much. Changing the pressure and thereby the velocity has a significant influence on the distribution only below the threshold of the nozzle. In this case, this point seems to be around 7.5 m s^{-1} or 1 bar. The figure also shows that lowering the velocity below this threshold creates a v-shaped distribution curve unsuitable for even distribution of water.

Figure 6.4: Distribution of water for variety of initial velocities and particles sizes. Nozzle height of 1 meter above the ground and spray angle of 55° .

The relation determined in this section gives the ability to calculate the maximum spraying distance of a nozzle as well as the distribution curve. This in turn gave insight into the dynamics of a nozzle and which parameters most affect the performance. A nozzle with smaller droplets has a more v-shaped distribution curve and lower max range compared to a nozzle with larger particles. The other parameter of influence was the initial velocity directly related to the pressure. If the pressure is above the threshold of the nozzle, the distribution of water is relatively constant. It can be argued that by increasing the velocity smaller droplets form which could affect the distribution of water. This, however has not been investigated in this study. The next part focuses on the design of the 400m spray cart and placement of the nozzles.

6.3 Design of 400m water spray cart

For the 400m long ice skating track, two water spray carts will be used in Winterswijk. The carts drive continuously around the track and are only removed from the track at the end of the night. To prevent freezing of the water nozzles, water is sprayed continuously during the night. To allow variation in the applied layer thickness and the amount of water sprayed per hour, the water pressure and cart velocity can be changed. Further flexibility is created with an additional set of nozzles for both carts. Changing the configuration of the nozzles on the cart allows for more or less water to be applied during that night. In this section a model is made for the 400m ice track to see how the pressure, cart velocity, and nozzle configuration affect the water flow rate and water layer height. The outer track of the 400m track has a longer distance compared to the inner track, this difference results in uneven distribution of water if the nozzles are spaced evenly. A design for redistributing the nozzles is made to counteract this affect while sustaining an even flow on the straight sections of the track.

6.3.1 Ice rink challenges

The ice skating rinks exists of two straight sections and two turns. The width of the track is ten meters and by the international skating regulations, the inner radius of the turn can vary between 25 meters and 26 meters. The outer side of the turn has a longer distance and so the cart has to travel faster to keep up. This will result in a reduced water layer height on the outer ring of the track. To get an estimate, if this will result in a problem, the area of the outer circle and inner circle are calculated by equations 6.3.1 and 6.3.2. With R_c the radius of the center line and W the width of the track in meters. The results of this combined with the inner and outer length of the tracks are presented in table 6.1.

$$A_i = 0.5\pi(r_c^2 - (r_c - \frac{w}{2})^2) \quad (6.3.1)$$

$$A_o = 0.5\pi((r_c + \frac{w}{2})^2 - r_c^2) \quad (6.3.2)$$

Table 6.1: Area and length of the inner and outer region of the turn.

	Area (m^2)	Length (m)
Inner	432	157
Outer	511	220
Ratio	1.18	1.4

From the table, its clearly visible that the cart has to travel significantly faster along the outer ring and thus less water is sprayed per meter. To get a uniform spray pattern along the entire turn an extra tube with nozzles can be placed along the arm of the cart. This is then only turned on while the cart is in turn. Or the nozzles can be placed closer together further from the centre to compensate for the velocity of the cart. A closer look is taken on the last option because its most economical and no extra control system is needed. First a closer look is taken for the overall layer height difference between the straight and turn sections of the track.

6.3.2 Turn compensation

The cart has a constant velocity along the inside of the track, therefore the time it takes to complete a full turn is equal to the inner turn length in a straight line. However, the outside of the cart has to move faster as shown above so less water is sprayed and a lower layer height is obtained, the derivation below shows how much difference there is between a straight section and the curve of the ice rink. Figure 6.5 shows the area of the road in grey with the dimensions as used earlier.

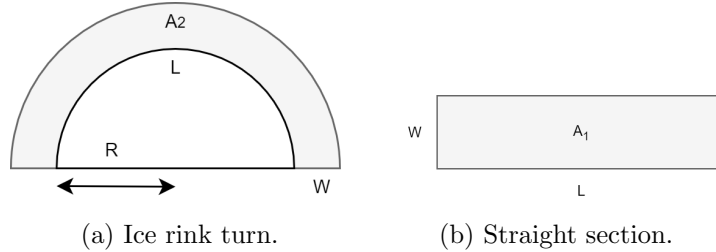


Figure 6.5: Schematic of the ice rink turn and straight section with inner length of the circle being equal to the length of the straight.

The area of the straight and curved sections are presented in equation 6.3.3 and the ratio between these are rewritten in equation 6.3.5 to obtain the simple formula of $\frac{w}{2r} + 1$ and with an inner radius of 25 m and width of 10 m the ratio $\frac{A_2}{A_1}$ becomes 1.2. In the case that the water spreads out evenly over the turn, the turn would need an extra pass by the spray cart every five laps to compensate for the reduced layer height. In practice, this difference in layer height might not be noticeable because it is over a large section of the track.

$$A_1 = \pi r w \quad (6.3.3)$$

$$A_2 = ((r + w)^2 - R^2) \frac{\pi}{2} \quad (6.3.4)$$

$$\frac{A_2}{A_1} = \frac{((r + w)^2 - R^2) \frac{\pi}{2}}{\pi r w} = \frac{w^2 + 2wr}{2wr} = \frac{w}{2r} + 1 \quad (6.3.5)$$

6.3.3 Redistributing the nozzle location

By rearranging the positions of the spray nozzle on the cart the lower layer height could be compensated. To understand the effect this has, a model has been made in Matlab to see the effect of changing the location of the nozzles. Three different configurations are presented throughout this model, the first with an even distance between nozzles along the cart, second configuration with the nozzles spaced to compensate for the turn, and the last with a mix between the first two.

The track curve can be split into N_s section with equal area A_s and with equation 6.3.6 the start and end radius of each section can be calculated with r_i being the inner radius of the track. For the third configuration, the area of the section is reduced for the inner turns and increased further outwards to get a new configuration in the middle. In figure 6.5a the width of each section is presented, which shows a large difference between the inner and outer turn for a turn optimised layout.

$$r_i = \sqrt{\frac{2A_s}{\pi} + r_{i-1}^2} \quad (6.3.6)$$

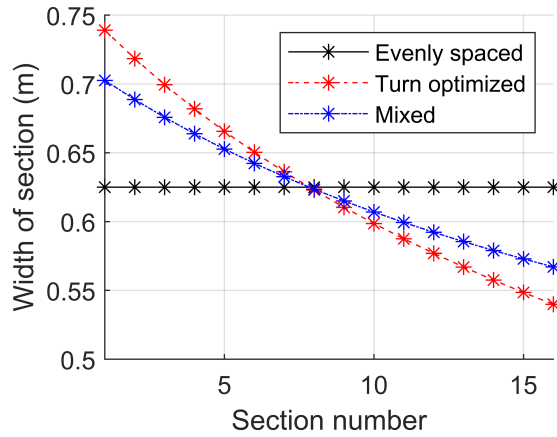


Figure 6.6: Spacing between each section for the different configurations.

While the second configuration is optimal for spraying an even layer of water in the curve of the ice rink. The entire track should be sprayed as evenly as possible. To get a better understanding of this, two figures are presented which show the layer height for each section. In this example the width of the track is taken to be 10 meters with 16 nozzles along the radius of the track. The results of this are presented in figure 6.7 with the layer height of the turn as the baseline and set to unity. The y-axis shows the deviation from this average with on the x-axis the location along the cart as seen from the centre point of the turn.

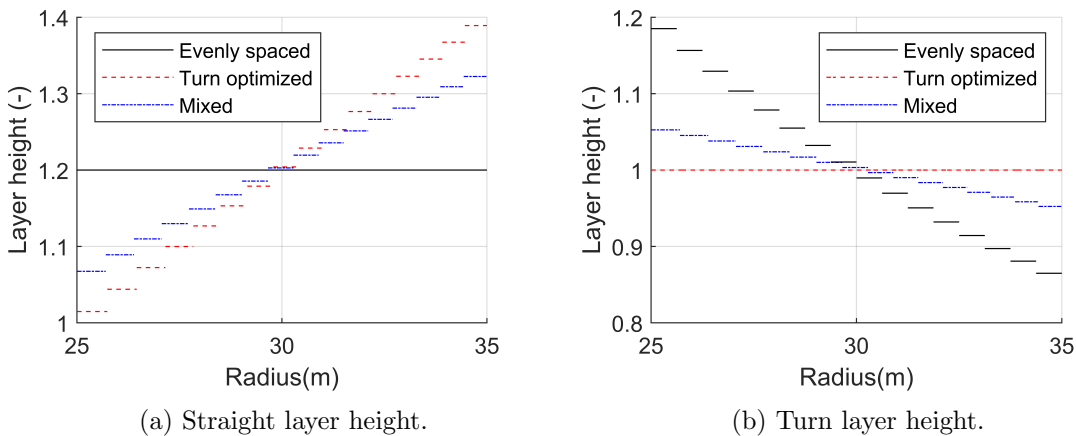


Figure 6.7: Layer height normalised by the average layer height in the turn.

As expected the evenly spaced nozzles perform the best on the straight section and the turn optimised spacing performs the best in the turn. However, the most interesting part is the additional configuration which performs slightly worse on the straight section but greatly improves the performance in the turn. Where as the evenly spaced configuration has a water layer that is 20% thicker in the inner curve than average. The new configuration only has a 5% thicker water layer. This shows that altering the spacing between nozzles could improve the distribution of a layer of water.

6.3.4 Total water flow rate

The carts drive continuously spraying water to avoid freezing of the nozzles, thus limiting the water flow rate by turning of the pump is not an option. Flexibility in the water flow rate is created by either changing the selections of nozzles, reducing the number of carts, or changing the pressure. Each cart has the ability to fit sixteen nozzles. Because two sets of nozzles are available, the most

common configuration would be to use the cart with only one type of nozzle or in between with eight small and eight large nozzles. The nozzle configuration is denoted with an ratio, $R = 0$ meaning completely fitted with small nozzles and $R = 1$ means, fitted with only the larger nozzle type. The flow rate for a nozzle depends on the water pressure as seen in 6.1.4 by using the flow rate versus pressure data from the manufacture, the total flow rate for cart can be calculated and is denoted with the symbol \dot{Q}_{cart} . With the number of carts N_{carts} , the ice rink area A , pressure P , and nozzle ratio R the thickness the water layer can be calculated as seen in 6.3.7 with h_{hour} the height of the water layer after a single hour.

$$h_{hour} = \frac{3600N_{carts}\dot{Q}(P, R)_{cart}}{A} \quad (6.3.7)$$

The relation is plotted in figure 6.8 with on the x-axis the water inlet pressure in bar and on the y-axis the water height increase in mm per hour. The individual lines correspond to three different nozzle configurations.

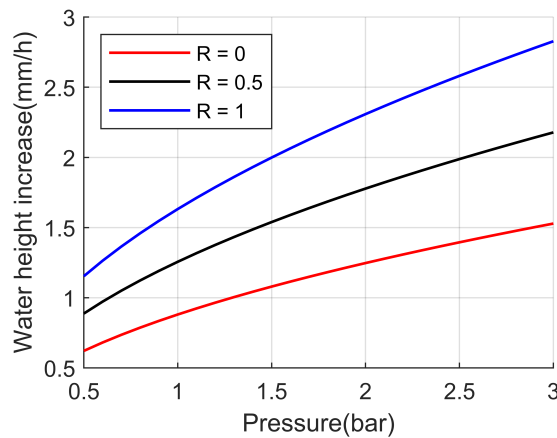


Figure 6.8: Water height per hour for different nozzle configurations and pressure on the 400m ice track. Using two spray carts.

6.3.5 Water layer height

With the total water flow rate known it is now possible to calculate the layer height. By increasing the velocity V_{cart} of the spray cart the time between each layer t_{layer} reduces. Time between each layer is calculated using equation 6.3.8 with the L the length of the track, set to 400m. When using the second spray cart the time between a layer is reduced by an factor of two.

$$t_{layer} = \frac{L}{N_{carts}V_{cart}} \quad (6.3.8)$$

The total height of the water layer applied is calculated with volume divided by area. The water volume equals the time for a layer and the flow rate of the carts. The equation is shown in 6.3.9, the only independent parameters are pressure, nozzle ratio, and cart velocity. From this conclusion it follows that the layer height is independent from the number of carts on the track, only the time between a layer is affected.

$$h_{layer} = \frac{t_{layer}N_{carts}\dot{Q}(P, R)_{cart}}{A} = \frac{L\dot{Q}(P, R)_{cart}}{AV_{cart}} \quad (6.3.9)$$

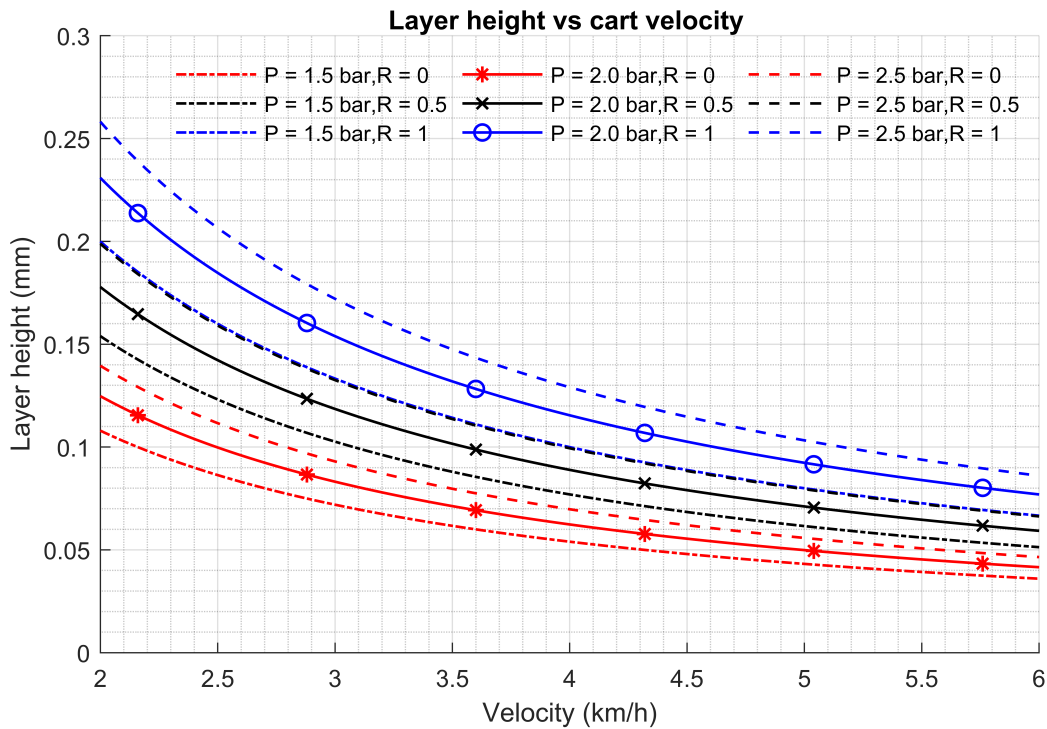


Figure 6.9: On the y-axis water layer height and on the x-axis cart velocity. Using three distinct nozzle ratios and three different pressures.

The relation is plotted in figure 6.9 with the water layer height on the y-axis and the cart velocity on the x-axis. In the figure three different nozzle ratios are plotted with the red line for $R = 0$, the black line for $R = 0.5$, and the blue line for $R = 1$. The dash-dotted line is used for a pressure of 1.5 bar, solid line for a pressure of 2 bar and the dashed line for a pressure of 2.5 bar. A full scale figure is presented in appendix C.1.

6.4 Final design

The skating association in Winterswijk has constructed two spray carts for the 400m track. The final spray cart is visible in figure 6.10. The design has a place for sixteen nozzles and each cart has two sets of nozzles allowing for easily changing the total flow rate. The nozzles are placed closer together on the outside of the turn as discussed to achieve an uniform layer of water during spraying. The first tests with the spray cart have been successful on January 31. The 400m ice track in Winterswijk was able to open the doors, and welcome the first ice skaters.[2][25]. Even though there was a curfew, an ice floor with a thickness of 4mm was created during only a single morning. The ice skating association was more than happy with the obtained results and quality of the ice.



Figure 6.10: Spray cart in use on the 400m ice track in Winterswijk.

6.5 Conclusion

This section has focused on the spray carts constructed in Winterswijk. An flat spray nozzle has the most uniform profile and allows for fine adjustments by turning the nozzle. This type has been used in all three spray carts in Winterswijk. By using the equation of motion of a water droplet, the factors influencing range and distribution of water have been examined for a flat spray nozzle. The model showed that reducing the pressure below the nozzle threshold in this case 1 bar. The range and uniformity of the nozzle is greatly reduced. If the pressure is above the threshold only, the range is slightly increased. The droplet size influences the distribution significantly, larger droplets are less affected by drag. The result of this is that a small size droplet has a lower range. In this study, the effect of increasing pressure and velocity on the particle size has not been investigated. It is expected that with an increased pressure, particles more easily break apart and create a finer mixture of particles. This in turn could affect the max range of the nozzle.

Chapter 7

Ice growth via spraying of multiple water layers

In this chapter, the outcome of the ice growth experiment conducted at the University of Twente is presented and discussed.

7.1 Introduction

The objective of this study was to research methods to improve the usability of an natural ice skating rink and in particular for the newly built ice skating rink in Winterswijk. The association in Winterswijk will use a spray cart as seen in the previous chapter to create an ice floor. Conventional method used by other ice skating associations is flooding the entire ice track with a layer of water just before a cold night. An advantage of using a spray cart compared to flooding the ice track is the ability to stop at anytime. If, for example, the conditions during the night are not enough to completely freeze the flooded track, a water layer will be trapped beneath the ice, thereby making the ice track unusable or of poor quality. Besides this, a spray cart allows for an additional layer of water to be added during the next night, increasing the ice thickness. The spray cart allows to set the flow rate of water over the track as well as the interval for a new water layer. On of the questions asked by the ice skating association in Winterswijk is whether there is an optimal setting for creating an ice floor. After dialogue with other ice skating associations in the Netherlands, the majority agreed that its best to have as small as possible layers of water to increase the ice floor yield. This lead to the following question, which will be answered in this chapter: "What is the effect of the water layer height on the ice growth rate?". To be able to answer this question, an experimental setup was constructed at the University of Twente. This chapter is structured as follows: sections two and three describe the hypothesis and the method of experimenting, after this section four and five explain the experimental setup, this is followed by the calculations and results in section five and six and this chapter is concluded in section seven.

7.2 Hypothesis

The ice floor in Winterswijk will be created by periodically spraying water, this gives the question: "Is it beneficial to periodically spray a thick layer of water, or thin layers of water with a higher frequency?. Or in other words, does the layer height influence the freezing rate. After applying a layer of water, its losses heat to the surroundings as well as by conduction to the ice below. This is because initially the new layer of water has a higher temperature than the ice. However, the only way of ultimately subtracting heat from the system is by transferring heat away from the top surface to the surroundings, by either convection or radiation. The higher the temperature

difference between the surface and the surroundings, the higher the heat fluxes. On the other hand, if the surface of the ice has a high temperature for a long period of time, the heat is able to penetrate deeper into the ice floor. This in turn will need more time to cool down while the heat conducts back to the surface. In addition to this, it is expected that ice will grow from the top surface downwards for large layers, this in turn creates an insulating layer between the remaining water, thus slowing down the rate of freezing. The hypothesis is that a thin layer of water will conduct less heat further downwards into the ice floor as well as have a thinner insulating ice layer at the top surface. To conclude, ice growth is faster when periodically spraying several thin layers with a high frequency compared to a single thick layer.

7.3 Setup

To be able to grow ice in a controlled manner, an experimental setup is created to simulate the heat loss through radiation as would normally happen towards the night sky. The setup is build around an insulated PVC tube with dimensions of 125x3.2mm and height of 200mm. Cold plates are placed at both ends of the tube to control the temperature of the simulated open night sky and the ground temperature below the ice. With the use of the pulse-echo method the thickness of the ice can be measured without interfering with the experiment. Figure 7.1 shows a schematic drawing of the setup. From the bottom to the top, first the transducer needed for the ice thickness measurement and the cold plate which supports the PVC tube. The surrounding of the tube is insulated with a layer of glass wool to prevent heat loss to the surroundings, which would otherwise influence the experiment. An connection has been made near the bottom surface where a PT100 temperature sensor is fitted into the reservoir. Along the side, an additional connection is made where a water tube is fitted. The flow of water is controlled by a peristaltic pump which is able to precisely dispose water. The top is closed with another cold plate which is insulated on the top surface and is meant to simulate the open night sky. The final setup is shown in figure 7.2.

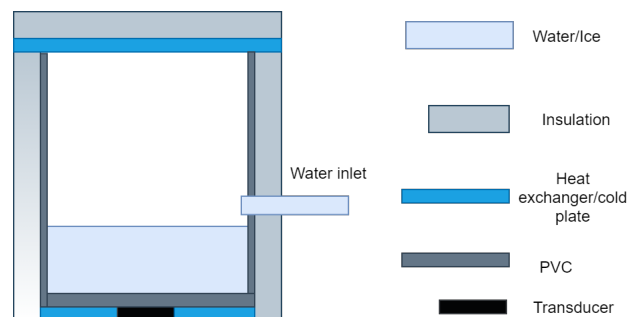


Figure 7.1: Schematic drawing of the experimental setup.

7.4 Method

The experiments were conducted during the period from September till October 2020. In the weeks prior, the experiment setup was constructed, tested, and improved. To answer the research question, several different water layer height have been selected and tested, these are: 0.72mm, 1.44mm, 2.88mm, and 5.76mm. Demineralized water is used for the experiment and the water is boiled before to extract gas from the water to avoid the formation of air bubbles during freezing. At the start of the experiment, the cryostat is cooled down to -20°C and the domestic cooler to -1°C . These temperatures are used for all experiments unless specifically stated otherwise. The container in which the ice grows is clamped between both cold plates to ensure a tight fit to minimise heat loss by air leakage. After both coolers settle to the set temperature, water is sprayed every 1, 2, 4, or 8 hours. These spray intervals correspond to four different layer heights, with the smallest layer

corresponding to the smallest interval. During the experiment, the temperature of the water inside the reservoir is measured as well as the domestic cooler temperature, which supplies the cold glycol for the bottom plate. The data of the oscilloscope is saved every few seconds and used to determine if the water is frozen and measure the thickness. In the following section the different components of the experimental setup are discussed in more detail.

7.4.1 Ultrasonic pulse-echo method

The pulse-echo method is a non-destructive testing technique which uses ultrasonic waves to find either defects in materials or measure the thickness of a specimen. The set-up of the ultrasonic equipment consists of a pulse generator which sends an electric pulse to the transmitter probe, which then produces an ultrasonic echo. This wave spreads itself around the specimen and is reflected to the receiver. The electronic signal from the receiver is sent to an oscilloscope which displays the signal. With on the vertical axis the amplitude of the signal and on the horizontal axis the time. Depending on the velocity of sound in a material and the travel time of the echo, the travel distance of the echo can be calculated. Often times more echoes are visible while having the same physical distance. Those echoes arise because only part of the wave enters the receiver probe and the other part is reflected. The intensity of the wave reduces while travelling through the material due to scattering, thereby reducing the amplitude of the peaks further in time. As signal generator an Olympus 5072PR is used which sends and receives the signal to the transducer. The equipment also amplifies the signal before sending it to the Fluke PM3394A oscilloscope. The oscilloscope has a fixed resolution of 512 data points, because a higher accuracy is needed, the interval region is split in several intervals each with 512 data points. Combining these intervals delivered a wide range signal in high resolution, but added more complexity in the data analysis phase.

7.4.2 Cold plate

The top and bottom side have a cold plate with a thermal resistance of $0.038\text{ }^{\circ}\text{W}^{-1}$ at a flow of 3.78 L/min. The top side of the setup is cooled to $-20\text{ }^{\circ}\text{C}$ with a FP35-HL refrigerated circulator and with a pump capacity of 22 l/min more than capable to achieve accurate temperatures at the top plate surface. Because only one refrigerated circulator is available, a domestic cooler is used for the bottom side of the setup. During testing, the beer cooler showed a larger fluctuation about the set point temperature and this caused various problems later on during the experiment. This problem is discussed in more detail in the discussion section.

7.4.3 Peristaltic pump

To add a new layer of water to the setup automatically, a peristaltic pump is turned on for a set amount of time. Operating the peristaltic pump was done by using a NodeMCU board (microprocessor), connected to the internet by WiFi allowing to change the settings while operating. This microprocessor controlled a relay which was connected to the peristaltic pump and an 12V power supply.

7.4.4 Temperature sensor

Temperature measurements are obtained by using two PT100 elements. The first on the bottom side cold plate which is connected to the beer cooler. The other is placed inside the tube near the bottom surface. Allowing to measure the temperature of water or ice during the experiment.

7.4.5 Final setup

The final experimental setup, for the ice growth experiment, is shown in 7.2. Visible on the left is a cryostat supplying a glycol mixture cooled down to $-20\text{ }^{\circ}\text{C}$ to the insulated top cold plate. Below

the top cold plate is the PVC tube where the water is injected. On the right side of the image are the oscilloscope, temperature measurement equipment and signal generator visible from bottom to top.



Figure 7.2: Photo of the final ice growth setup.

7.5 Calculations

In this section calculations are made to estimate how the experimental setup relates to the outside ice growth conditions. In the last part the necessary equations used in the ice thickness measurements are explained.

7.5.1 Heat transfer

The modes of heat transfer inside the reservoir are conduction and thermal radiation, the assumption is made that natural convection is not significant inside the closed cylindrical tube due to the low velocity. First, the energy transfer via conduction through the side wall is calculated. The internal temperature (T_i) is taken to be the freezing point of water (0°C) and the ambient temperature (T_a) is taken to be 20°C . Heat transfer by conduction through the walls of the cylinder follows from equation 7.5.2 where R is the thermal resistance of the PVC wall and glass wool insulation. The thermal resistance is calculated with equation 7.5.1. The thermal conductivity is denoted with k and the thickness of the layer with L . The outer radius r_2 and inner radius r_1 .

$$R = \frac{\ln(r_2/r_1)}{2\pi kL} \quad (7.5.1)$$

$$Q_{Side} = \frac{T_i - T_a}{R_{PVC} + R_{Insulation}} \quad (7.5.2)$$

The resulting energy loss with a temperature difference of 20°C is 0.0671 W over the entire wall of the cylinder, because only a fraction of the wall will be in contact with the ice. This term is negligible and shows that the isolation is adequate. The heat transfer from the bottom cold plate to the new layer of water is calculated with equation 7.5.3 where T_b is the bottom cold plate temperature. The thermal resistance is now calculated with the relation for a flat plate shown in equation 7.5.4.

$$Q_{Bottom} = \frac{T_i - T_b}{R_{PVC} + R_{Ice}} \quad (7.5.3)$$

$$R = \frac{kL}{A} \quad (7.5.4)$$

If the internal temperature is again considered as a fixed value at the freezing point of water. The heat transfer from the bottom cold plate depends on both the temperature of the cold plate and the ice thickness. Figure 7.3 shows the relation plotted for three different cold plate temperatures. The resulting plotted lines clearly show that the cold plate temperature has a significant influence on the freezing rate of the ice, varying from 60 W m^{-2} to 130 W m^{-2} .

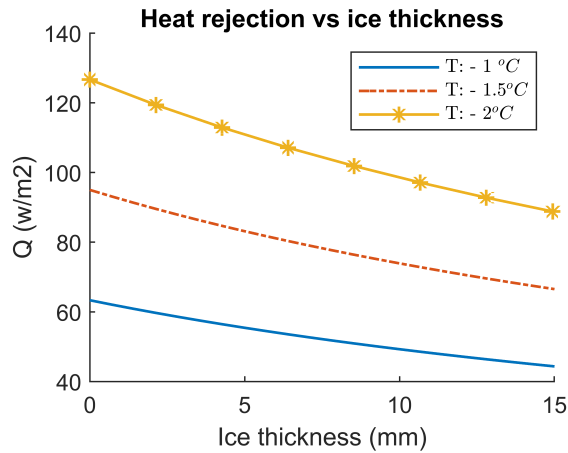


Figure 7.3: Heat rejection from the bottom cold plate against ice thickness, for different cold plate temperatures.

The next mode of heat transfer discussed is thermal radiation, this form of heat transfer is slightly more complex due to the fact that there are three surfaces radiating. Therefore, the correct view factors are needed to calculate the net heat transfer, a first assumption is made to simplify the problem. This assumption states that the sides of the cylinder are the same temperature as the ice, resulting in zero net heat transfer between the ice and the sides of the cylinder. For ease of use, the surfaces of the cylinder are numbered the following: surface 1 is the layer of water/ice, surface 2 are the walls of the cylinder, and surface 3 is the top surface of the setup. Relations for the view factors are obtained from the catalogue of radiation configurations [26]. The relation shows that for the used cylinder dimensions only 7.5% of the thermal radiation from surface 1 is directed to surface 3. With the cryostat set to an temperature of -20°C the resulting heat loss from the ice is only 6.2 W m^{-2} . In comparison, thermal radiation to the sky at a surface temperature of 0°C varies from 0 W m^{-2} for cloudy conditions to 80 W m^{-2} for open skies. The ability to loss heat by radiating is thus limited inside the experimental setup compared to outside conditions. On the other hand, the heat transfer through the bottom cold plate is 62 W m^{-2} in the case of no ice present and a bottom cold plate temperature of -1°C . This indicates that care should be taken while setting the temperature of the bottom cold plate.

7.5.2 Ice thickness

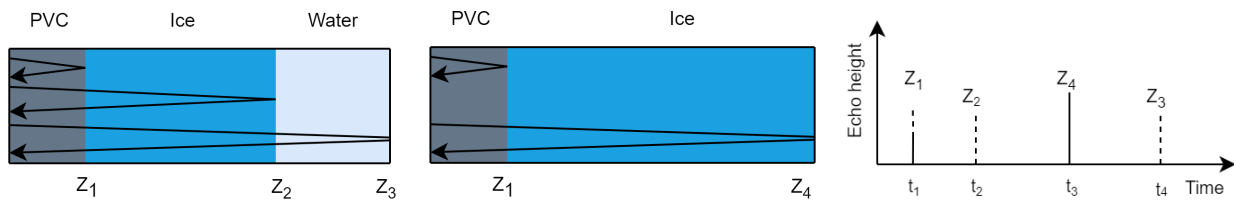
The ice thickness setup relates the output signal from the oscilloscope to an estimated ice thickness. After sending an electronic pulse to the transducer, a sound wave travels through the specimen, reflecting on each interface it passes through. The delay between sending and receiving the reflected echo wave is called the wave transit time. The transit time gives the distance to the interface when

the sound velocity is known. For example: in water, with the velocity of sound $v \approx 1402 \text{ m s}^{-1}$, the wave travels through 20 mm in a time of $t = 14.3 \mu\text{s}$. The distance of the interface away from the transducer x is half the travelled distance. The relation is shown in equation 7.5.5. The amplitude of the echo intensity is referred to as the echo height and depends on the acoustic impedance ratio between the materials. A large difference in material impedance results in a large reflection coefficient. The water-air interface is an interface that has a large difference in acoustic impedance. As a result of this, it is usually a perfect reflector of ultrasonic waves.

$$t = \frac{v}{2x} \quad (7.5.5)$$

Figure 7.4a shows the configuration after applying a layer of water on the ice. The first interface is between the PVC and ice (Z_1), the second interface is between ice and water, (Z_2) and the last interface is between water and air (Z_3). In the second figure 7.4b the configuration is shown when completely frozen. The first interface between PVC and ice is still intact, the interface between ice and water disappeared, and a new interface between ice and air is formed (Z_4). The path an echo travels through the material is denoted with an arrow, each arrow corresponds to a peak on the oscilloscope. The expected output for both cases on the oscilloscope is displayed in figure 7.4c, the dashed lines show the peaks as would be visible after applying a layer of water. The solid lines show the peak after the reservoir is completely frozen. The peak of interface Z_2 moves to the right with time and the peak of interface Z_3 moves to the left with time. By keeping track of how much water is in the the reservoir, it is possible to determine the expected location a peak is visible when completely frozen. This expected location or echo transit time is the combined time it takes to travel through the PVC layer and the ice layer, as shown in equation 7.5.6. The inverse is also possible and allows to determine the thickness from the transit time. If a peak is present at the time of t_4 , the ice is assumed to be completely frozen, allowing to calculate the time to freeze for this layer.

$$t_4 = \frac{v_{pvc}}{2x_{pvc}} + \frac{v_{Ice}}{2x_{Ice}} \quad (7.5.6)$$



(a) Configuration of the layers after applying a layer of water.

(b) Configuration of the layers when completely frozen.

(c) The expected output signal, the stripped lines is for the configuration seen in figure 7.4a and the solid lines for the configuration seen in figure 7.4b.

Figure 7.4: The principle of the pulse echo ice thickness method. The arrows indicate the path of an echo. Z_i is used to denote an an interface between two materials.

7.6 Results

In this section the results of the experiment are presented. The data from the ice thickness setup showed to be inconsistent and highly fluctuating for real-time ice growth rate measurement. However the ice thickness setup was able to determine if there is an interface between ice and air as seen in figure 7.4b, this is the case when the water is completely frozen. The setup determines if the water is completely frozen based on the condition that there is a high intensity peak near the expected location of the ice-air interface. The expected peak location is determined by equation 7.5.6. Figure 7.5 schematically shows the echo height over time for the duration of a layer. At first, there is no interface to reflect on, so the line is horizontal. At the moment the water completely freezes, the ice-air interface is completed and the ultrasonic waves reflect on this, thereby increasing the echo height. The moment this happens is the time-to-freeze for that specific layer. This output is fitted to a sigmoid curve with the midpoint of the sigmoid curve as the time-to-freeze, the midpoint line is shown in figure 7.5. If the midpoint shifts to the right, the time-to-freeze increases and vice versa. The time-to-freeze and layer height is used to calculate the freezing rate of the water layer, the output data of this is presented in figure 7.6. Sigmoid curves for all layers are plotted in appendix A.1.

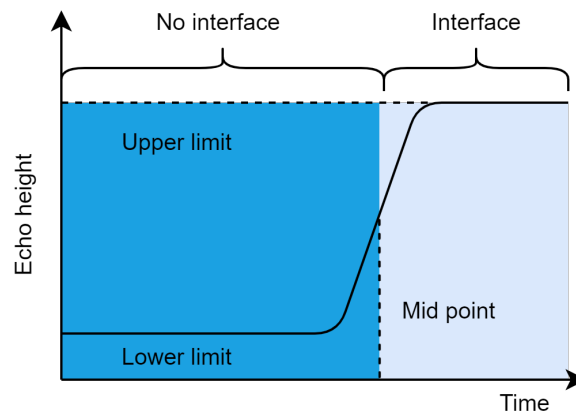


Figure 7.5: Principle of determining ice-air interface.

Figure 7.6 shows the freezing rate on the y-axis in mm per hour and the four different spray intervals, corresponding to the four different water layer heights. For the one-hour interval, sixteen layers are created, two-hour interval ten layers, four-hour interval four, and eight-hour interval three. The limited number of data available for the longer layers allows for a wide spread of freezing rates. The limited number of data points and the implication this has are discussed more in depth in the next section. The freezing rate for a one-hour period varies from 1.04 to 1.29 mm/h in the first quartile. For a spray interval of two hours and double water layer height, the freezing rate varies from 0.97-1.25 mm/h. For the four-hour spray interval, the measurements were inconclusive and showed a wide spread, the cause of this is unknown. The freezing rate varies from 1.01 to 1.6 mm/h. The longest water spray interval of eight hours has a freezing rate between 0.73 to 0.91 mm/h. It should be noted that two of the layers in the experiment have a freezing rate of 0.73 mm/h, the third strongly deviates from this with 0.91 mm/h. Excluding the data points from the four-hour water spray interval, there seems to be a general trend that a shorter water spray interval corresponds to a higher freezing rate.

7.7 Discussion

During the design, building and testing of the experimental setup, several challenges unfolded. A selection of these challenges is discussed here and should be taken into account for further research

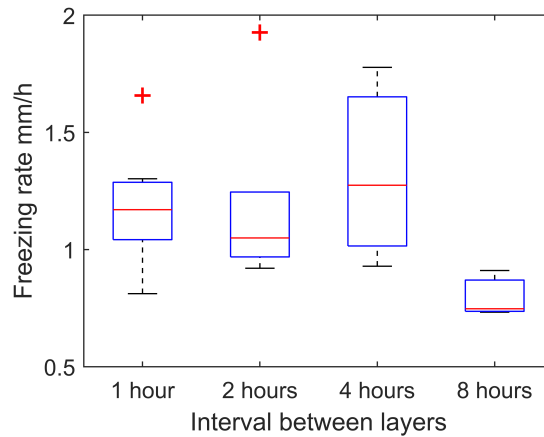


Figure 7.6: The freezing rate versus the layer interval duration.

on a similar setup. The main challenge of the design was being able to measure the thickness of a layer of ice without needing to stop the experiment. The final design uses the pulse echo method to measure the ice thickness, a method also used to find defects in materials. Even though this method works, it generates a lot of data which needs additional processing compared to a simple temperature sensor, it is not as reliable. For example, the formation of air bubbles in the ice scatters the sound wave, making it not possible to obtain a signal. This problem was reduced by using demineralized water and boiling before use to reduce the dissolved gases in the water. Further research should focus on finding a method to improve reliability. The decreased reliability and the duration it takes to do an experiment resulted in the limited number of data points. The limited available data has the implication that the freezing rate is widespread, making it not possible to indicate anomalies. This is especially the case for the four and eight-hour layer interval with only three data points. Excluding the four-hour layer height data, there seems to be a slight trend indicating that larger time between layers, reduces the freezing rate. This answer to the research question should be taken with caution as the data is limited and the temperature of the domestic cooler showed to be inconsistent. The domestic cooler used for the bottom cold plate was not able to sustain a constant temperature throughout the experiment. The resulting ice growth rate difference between the different experiments might come from this inconsistent temperature, instead of the difference in layer height. The experimental setup was meant to simulate thermal radiation towards the night sky, however the calculations showed that the major loss of heat happens through the bottom cold plate. This has the result that the direction of ice growth is flipped as to stated in the hypothesis, the ice now grows from bottom to the top.

7.8 Conclusion

The objective of the experiment was to determine if there is a higher ice growth rate when spraying multiple layers of water compared to a single thick layer of water. If this is the case the ice association in Winterswijk can focus on spraying thin layers of water during the night to increase the yield of ice. During the experiment, four different water layers height are tested. These layer heights are 0.72mm, 1.44mm, 2.88mm and 5.76mm corresponding to a layer interval of 1, 2, 4 and 8 hours. The smallest layer height had the fastest freezing rate varying from 1.04 to 1.29 mm/h, the second fastest freezing rate was seen in the 2 hour layer interval with freezing rate varying from 0.98 to 1.25 mm/h. While the data for larger water layers indicate to a lower freezing rate, the data is widespread and inconsistent. In addition to this, the temperature of the bottom cold plate was not able to be constant throughout a single layer and overshadowed the heat rejection by thermal radiation. The hypothesis was based on the fact that an insulating layer of ice would form on the

top surface, reducing net heat rejection, thereby limiting ice growth. However the bottom cold plate was the largest heat sink and the ice growth direction was flipped in the setup. The ice grows from bottom to the top, consequently there is no top surface to insulate the water. This makes part of the hypothesis invalid. These factors combined make it impossible to conclude the results. Further research in a better controlled environment is necessary to answer the research question. While the experiment failed to answer the question if smaller thinner layers of water layers freeze faster. The concept of using the pulse echo method to measure the moment ice freezes without disrupting the experiment proved to be possible and could be built upon in further research.

Chapter 8

Discussion

The objective of this study is to gain insight in the design of an efficient natural ice skating rink. Due to global warming, only a few days in the year have temperatures that allow ice growth. Even fewer days in the year allow for ice to grow thick enough to support the weight of an ice skater on open water. The use of an ice skating rink reduces the necessary thickness of the ice layer, thereby providing more people the ability to go ice skating. However, the way ice grows on a natural ice skating rink differs from the way ice grows on open water and current ice growth models are not directly usable. On open water, ice forms on the bottom of the ice, whereas on an ice skating rink the ice forms on the top. Limited literature is available about ice growth on ice skating rinks. This study tries to fill this gap in literature by combining the existing literature on ice growth on open water into an ice growth model that is suitable for estimating ice growth on a ice rink. This ice growth model can be used for estimating ice growth with a high spatial resolution and includes the ability of spraying water periodically. The gained insight into the ice growth on a natural ice skating rink will contribute to the development of new and innovating ice skating rinks and may increase the ability of using skating rinks more often in the future, even under the current global warming circumstances. In addition to the ice growth model, two experimental setups have been created, which will be discussed in the next section. The first experimental setup focused on the effects of insulating the ice rink floor and is used as verification for the ice growth model. The second experiment focused on the effect between the water layer height and the ice growth rate. In the last section, additional research focused on the spray carts used at the ice skating rink in Winterswijk will be discussed.

In the first experimental setup, the asphalt setup, the temperature of a small-scale ice rink floor has been measured for two different configurations, being a standard and insulated ice rink floor. The experimental data showed that the insulated configuration has a lower asphalt surface temperature compared to the non-insulated configuration. This lower temperature indicates a reduced energy flux from the ground in the insulated configuration, which would result in more ice growth. Based on the retrieved data from the experimental setup, the results are promising and indicate that insulation helps ice growth. The expectation is that during a period of frost, the non-insulated ice rink floor would lose even more heat due to an increase in thermal conductivity. This expectation is based on research performed by Penner (1970), which showed an increase in thermal conductivity with soil temperatures below freezing. This effect is expected to only be noticeable for the uninsulated configuration as the insulated configuration with foamed concrete is non-permeable to water. Unfortunately, a continued period of frost was absent during the time of the experiment, which could confirm this expectation.

The data of the first experimental setup, the asphalt setup, is used to verify the ice growth model. Due to the relative warm winter weather during the experiment, there is limited data on temperatures below freezing, and no data is available about ice growth. Therefore, the verification of

the model is based on the temperature profile throughout the ground. The model showed to be consistent with the experimental setup during the night. However, the model underestimated the asphalt temperature during days with clear skies, resulting in a discrepancy between the model and asphalt temperature. This discrepancy is caused by the fact that there is no accurate cloud coverage data available. The absence of cloud coverage data is a limitation for the verification of the model. Another limitation of the verification of the ice growth model is that the total heat flux is estimated from the ground temperature fluctuation, instead of measuring the different heat fluxes directly. Future research could focus on the different types of heat fluxes with the use of, for example, an pyranometer to separate the solar irradiance from the total heat transfer.

The following section will discuss the ice growth model and the results of the model. Results of the ice growth model showed that for a scenario where there is a sudden drop in ambient temperature, the ice floor configuration with insulation provided better conditions for ice growth. In addition, the option of using a thinner layer of asphalt showed to be effective in combination with insulation. Therefore, the optimal design of an ice skating rink floor should be focused on first adding an insulating layer beneath the asphalt and after that, reducing the asphalt thickness. While completely removing the asphalt is ideal for the creation of an ice layer, this would create new challenges. The foamed concrete layer is extremely brittle and needs a protective layer to be usable. Hence, the thickness of the asphalt layer is limited by the necessary thickness to provide a protective layer for the foamed concrete layer. Future research should focus on finding different building materials with low thermal conductivity, which are strong enough to protect the ice rink floor.

The model estimates the sensible and latent heat transfer with the surface temperature, ambient temperature, and wind velocity. An additional factor, which has not been taken into account in the model, is the atmospheric instability due to the surface roughness of the ice. Research conducted on the artificial ice growth of floating ice platforms showed that a higher surface roughness increased the ice growth rate [27]. Artificially increasing the atmospheric instability with the use of ventilation or changing the surface roughness is a possibility for enhancing heat transfer, although this may not be practical for an ice skating rink. In addition, it may also reduce the ice quality.

A limitation of the ice growth model is the assumption of equal density of water and ice. Due to this assumption, the estimated ice thickness is underestimated in the model as the density of water is used for both phases. Another limitation to this assumption is that there are no buoyancy forces simulated in the model, which could increase the heat transfer in the top water layer by the movement of water. Due to the thin layers of water involved, it is expected that the increase in heat transfer and effect on the entire model is limited. However, additional research is needed on this aspect.

The effect of varying the water spray layer height was simulated in the ice growth model. Results of the model showed that applying a thicker layer of water freezes faster, compared to several thin layers of water. However, the effect of an increased ice growth rate for larger layers was only noticeable if the newly applied layer was allowed to cool down below freezing temperature, which resulted in a lower total surface heat exchange during the layer time. Making sure that the ice floor is always "wet" resulted in no significant difference in ice growth rate between different water layer heights. The model assumes that the surface is completely horizontal and that water is not able to flood away. In reality, the ice floor has a slope and applying too much water could result in the removal of ice in the centre of the ice rink and allow for the formation of a water puddle near the sides. The effect of the slope and to which extent this influences the ice growth has not been investigated in this study.

The second experimental setup, the ice growth setup, investigated the effects between the water layer height and freezing rate in a controlled environment. Due to the temperature limit of the cryostat, only a small portion of the total heat transfer was caused by thermal radiation. Resulting in the ice growth to be dominated by heat transfer through conduction to the bottom cold plate. This limited the ability to simulate ice growth caused by thermal radiation. The ice thickness sensor setup showed to be inconsistent and unable to produce reliable results for real time ice thickness measurements. Future research should investigate different methods of ice thickness measurements. The additional inconsistent temperature of the bottom cold plate made it impossible to interpret the final results of the experiment. While the results are inconclusive, there seems to be a trend that larger layers of water freeze slower compared to several thin layers. This result is in direct contrast to the ice growth model, where a larger layer of water freezes faster. One of the differences between the model and ice growth setup is the place where the heat is rejected. In the case of the model, energy is rejected at the top surface and in the ice growth setup the energy is rejected through conduction to the bottom surface, resulting in a flipped ice growth direction. The difference in ice growth direction could be one of the reasons why the outcome of the experiment is inconsistent with the ice growth model. In addition to this, the experimental setup applies a layer periodically while the ice growth model applies a layer if the surface temperature is below the critical temperature, allowing a variable time between each layer. Future research is needed to change the experimental setup.

A small addition to this study is the droplet distribution model, which has been used for the practical implementation for the ice skating association in Winterswijk. The droplet distribution model provides insight into the dynamics involved in applying a layer of water and estimating the water distribution. Due to the scope of this research, the water droplet model has been simplified and did not take into consideration the effects of evaporation or the effect of wind. The model did show that smaller droplets are strongly influenced by drag and therefore wind should have been incorporated into the model. However, the results from the first test of the ice skating association are promising, since the ice skating association was the first and only association in the Netherlands to open the ice rink on the night of November 30 2020[2].

Chapter 9

Conclusion

This study provides additional insight into the design of a natural ice skating rink and the process of natural ice growth. Limited literature is available about ice growth on ice skating rinks. In this study, a new thermodynamic, time-dependent model for simulating ice growth on natural ice skating is developed, with the inclusion of ground heat transfer. This model, based on literature, forms an attempt to fill the gap in the literature on ice growth models suitable for ice skating rinks. The insights gained by this study, improve the development of innovative ice rink design, which will help the ice skating association to increase the number of ice skating days in the year. The additional ice skating days in the year are not only a benefit for the ice skating association, but it might also be a necessary development in combating the effects of climate change in the Netherlands on ice growth. Next section will discuss the conclusion of this study, which indicates the optimal design of a natural ice skating rink, based on the model and experimental data.

The ice growth model results provide the distribution of ice and ground temperature, as well as the ice layer thickness and the convective, radiative and conductive heat fluxes. The influence of atmospheric conditions, design of the ice rink floor, and spray water thickness on the rate of ice growth have been examined. The ice growth rate increases when air temperature decreases, the cloud cover decreases, and the wind speed increases. An ice floor design with an insulation layer beneath the asphalt has been shown to provide a higher rate of ice growth, compared to a standard configuration with mixed granulate beneath the asphalt. Reducing the asphalt thickness for a configuration with insulation showed to be beneficial for the ice growth rate. The minimum asphalt thickness is however limited by the required necessary strength to provide a protective layer. Additional research into other materials could further optimise the structure of the ice floor.

Results from the ice growth model showed that increasing the water spray thickness could provide an increase in ice growth rate if the top surface temperature is allowed to drop below the freezing point. However, if the water spraying cart applies a new layer just before the layer is fully frozen, the surface temperature is unable to drop in temperature and no significant differences in ice growth rate are visible. This result, shows the importance of keeping the ice surface "wet" throughout the ice growth process.

The experiment performed in this study on the effects of the water layer height, has been conducted in a controlled ice growth setup and showed to be challenging. This was due to the lack of time available in this research and the complexity of measuring the ice thickness without interference. Most of the challenges in the experimental ice growth setup stem from insufficient reliable data from the ice thickness measurement setup and the inconsistent temperature of the setup. An optimised setup and additional data will go a long way to tackling the uncertainties of the results. No conclusion can be made from the gained results.

During the research, the ice skating association of Winterswijk built two water spraying carts which are used to apply layers of water during a period with frost. The requirement of the ice skating association was to be able to apply a thin and evenly distributed layer of water. Therefore, a spray droplet distribution model was made to gain insight into the dynamics of a spray nozzle. The model showed that increasing the droplet velocity resulted in a wider and more even water distribution. Reducing the droplet size resulted in the water distribution moving away from the centre, creating a v-shaped water distribution. The effect of water droplet size on the water distribution showed to be significant and future research on estimating the droplet size and the effects of wind on the droplet trajectory is necessary. Additional research has been performed on the placement of the nozzles on the spray cart. To achieve an even distribution of water in the curves of the 400m track, the nozzles in the outer range of the curve are placed closer together. While there is no research data available yet on the flatness of the ice due to the lack of strong frost, the first results in Winterswijk showed promising results with a thin flat layer of ice.

While there is no extensive scientific data available from the newly built ice skating rink in Winterswijk, the ice skating association was able to obtain a 10mm thick layer of ice during the the last night of November with only limited frost. The significance of this is that this was the only natural ice rink with a layer of ice in the Netherlands that day. The use of the ice growth model on-site with a microcomputer would be a beneficial tool in the construction of an ice layer and could also provide a better prediction of the maximum obtainable ice thickness during the upcoming night. This would increase the efficient use of resources of the ice skating association.

Hence, the most optimal design of an ice skating rink should have a foamed concrete layer as a replacement for the mixed granulate layer and strive for a reduced asphalt layer thickness. This helps prevent the stored heat in the ground from transferring to the surface in the case of a sudden drop in ambient temperature. Creation of the ice layer itself should be done by applying layers of water with a spray cart. Thereby, focusing on the correct timing of when to apply a new layer, reducing the time the last layer is below the freezing temperature. For the design of an ice skating track, the placement of nozzles on the outer edge of the curve should be moved closer together as to obtain an even distribution of water.

Bibliography

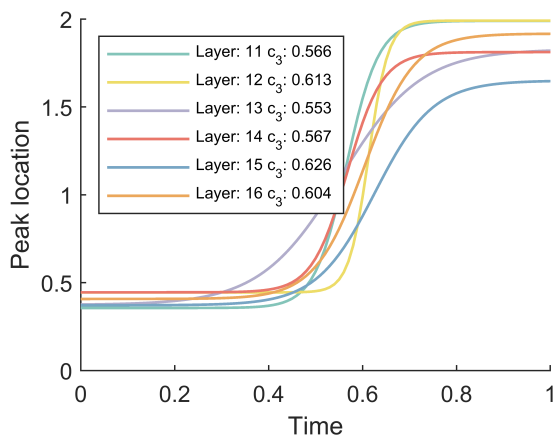
- [1] A Klein Tank et al. “KNMI ’14 Klimaatscenario’s voor Nederland”. In: (2015), p. 36. URL: www.klimaatscenarios.nl.
- [2] *Schaatsen op natuurijsbaan na één nacht matige vorst — Binnenland — Telegraaf.nl*. URL: <https://www.telegraaf.nl/nieuws/1420391536/schaatsen-op-natuurijsbaan-na-een-nacht-matige-vorst>.
- [3] Bernhard Harfsterkamp. *Een nacht vorst en al schaatsen in Winterswijk*. URL: <https://www.achterhoeknieuwsinterswijk.nl/nieuws/algemeen/335264/e-eacute-n-nacht-vorst-en-al-schaatsen-in-winterswijk>.
- [4] H. A. R. De Bruin and H. R. A. Wessels. “A Model for the Formation and Melting of Ice on Surface Waters”. In: *Journal of Applied Meteorology* 27.2 (Feb. 1988), pp. 164–173. ISSN: 0894-8763. DOI: 10.1175/1520-0450(1988)027<0164:amftfa>2.0.co;2.
- [5] J. Q. Keijman. “The estimation of the energy balance of a lake from simple weather data”. In: *Boundary-Layer Meteorology* 7.3 (Nov. 1974), pp. 399–407. ISSN: 00068314. DOI: 10.1007/BF00240841. URL: <https://link.springer.com/article/10.1007/BF00240841>.
- [6] George D Ashton. “Thin ice growth”. In: *Water Resources Research* 25.3 (Mar. 1989), pp. 564–566. ISSN: 0043-1397. DOI: <https://doi.org/10.1029/WR025i003p00564>. URL: <https://doi.org/10.1029/WR025i003p00564>.
- [7] Xing Fang, Christopher R. Ellis, and Heinz G. Stefan. “Simulation and observation of ice formation (freeze-over) in a lake”. In: *Cold Regions Science and Technology* 24.2 (1996), pp. 129–145. ISSN: 0165232X. DOI: 10.1016/0165-232X(95)00022-4.
- [8] Jouko Launiainen and Bin Cheng. “Modelling of ice thermodynamics in natural water bodies”. In: *Cold Regions Science and Technology* 27.3 (1998), pp. 153–178. ISSN: 0165232X. DOI: 10.1016/S0165-232X(98)00009-3.
- [9] *Crystal quartz (SiO₂) and Fused Silica*. URL: http://www.mt-berlin.com/frames_cryst/descriptions/quartz%20.htm.
- [10] Quirijn de Jong van Lier and Angelica Durigon. “Difusividade térmica do solo estimada por observações de sua temperatura e por propriedades dos seus componentes”. In: *Revista Brasileira de Ciencia do Solo* 37.1 (Jan. 2013), pp. 106–112. ISSN: 01000683. DOI: 10.1590/S0100-06832013000100011. URL: http://www.scielo.br/scielo.php?script=sci_arttext&pid=S0100-06832013000100011&lng=en&nrm=iso&tlng=en%20http://www.scielo.br/scielo.php?script=sci_abstract&pid=S0100-06832013000100011&lng=en&nrm=iso&tlng=en.
- [11] E. Øiseth, R. Aabøe, and I. Hoff. “Field test comparing frost insulation materials in road construction”. In: *Proceedings of the International Conference on Cold Regions Engineering*. 2007, p. 62. ISBN: 078440836X. DOI: 10.1061/40836(210)62.
- [12] Kevin Cavanaugh and Jeffrey F Speck. “Guide to Thermal Properties of Concrete and Masonry Systems Reported by ACI Committee 122”. In: *Concrete* (2002), pp. 1–21.

- [13] Robert Fajber, Adam H. Monahan, and William J. Merryfield. “At what time of day do daily extreme near-surface wind speeds occur?” In: *Journal of Climate* 27.11 (June 2014), pp. 4226–4244. ISSN: 08948755. DOI: 10.1175/JCLI-D-13-00286.1. URL: <http://www.cesar-database.nl>.
- [14] *Energy from the Sun - American Chemical Society*. URL: <https://www.acs.org/content/acs/en/climatescience/energybalance/energyfromsun.html>.
- [15] *Solar Radiation and Photosynthetically Active Radiation*. Mar. 2014. URL: <https://www.fondriest.com/environmental-measurements/parameters/weather/photosynthetically-active-radiation/>.
- [16] EFIMOVA and N. A. “On methods of calculating monthly values of net longwave radiation”. In: *Meteorol. Gidrol.* 10 (1961), pp. 28–33. URL: <https://ci.nii.ac.jp/naid/10006911925>.
- [17] JACOBS and J. D. “Radiation climate of Broughton Island”. In: *Energy Budget Studies in Relation to Fast-ice Breakup Processes in Davis Strait* (1978), pp. 105–120. URL: <https://ci.nii.ac.jp/naid/10006911942>.
- [18] Adrie F.G. Jacobs, Bert G. Heusinkveld, and Albert A.M. Holtslag. “Long-term record and analysis of soil temperatures and soil heat fluxes in a grassland area, The Netherlands”. In: *Agricultural and Forest Meteorology* 151.7 (2011), pp. 774–780. ISSN: 01681923. DOI: 10.1016/j.agrformet.2011.01.002. URL: <http://dx.doi.org/10.1016/j.agrformet.2011.01.002>.
- [19] Maximintegrated. “DS18B20 Programmable Resolution 1-Wire Digital Thermometer DS18B20 Programmable Resolution 1-Wire Digital Thermometer Absolute Maximum Ratings”. In: 92 (2019), pp. 1–20.
- [20] A. L. Buck. “New equations for computing vapour pressure and enhancement factor.” In: *Journal of Applied Meteorology* 20.12 (1981), pp. 1527–1532. ISSN: 08948763. DOI: 10.1175/1520-0450(1981)020<1527:necvp>2.0.co;2. URL: <https://ui.adsabs.harvard.edu/abs/1981JApMe..20.1527B/abstract>.
- [21] Yunus A. Cengel and Afshin J. Ghajar. *Heat and Mass Transfer, Fundamentals & Application, Fifth Edition in SI Units*. Vol. 5th. 2015.
- [22] *MC3E FLAT SPRAY NOZZLES - Euspray*. URL: <https://www.euspray.com/en/products/nozzles/flat-spray-nozzles/m-c3-m-c3e-flat-spray-nozzles/>.
- [23] Peter Timmerman and Jacobus P. van der Weele. “On the rise and fall of a ball with linear or quadratic drag”. In: *American Journal of Physics* 67.6 (1999), pp. 538–546. ISSN: 0002-9505. DOI: 10.1119/1.19320.
- [24] *Drag of a Sphere*. URL: <https://www.grc.nasa.gov/www/k-12/airplane/dragSphere.html>.
- [25] *Eerste schaatser op flinterdun natuurijs in Friesland en zelfs op 4,5 millimeter in Winterswijk — Binnenland — AD.nl*. URL: <https://www.ad.nl/binnenland/eerste-schaatser-op-flinterdun-natuurijs-in-friesland-en-zelfs-op-4-5-millimeter-in-winterswijk~a5e021bf/>.
- [26] John Howell. *A catalog of radiation configuration factors*. New York ; Toronto: McGraw-Hill Book, 1982. ISBN: 9780070306066.
- [27] K. Szilder and E. P. Lozowski. “Optimizing the growth thermodynamics of artificial floating ice platforms”. In: *Ocean Engineering* 16.1 (Jan. 1989), pp. 99–115. ISSN: 00298018. DOI: 10.1016/0029-8018(89)90045-0.
- [28] Matthew R Hall et al. *Influence of the thermo-physical properties of pavement materials on the evolution of*. Tech. rep.

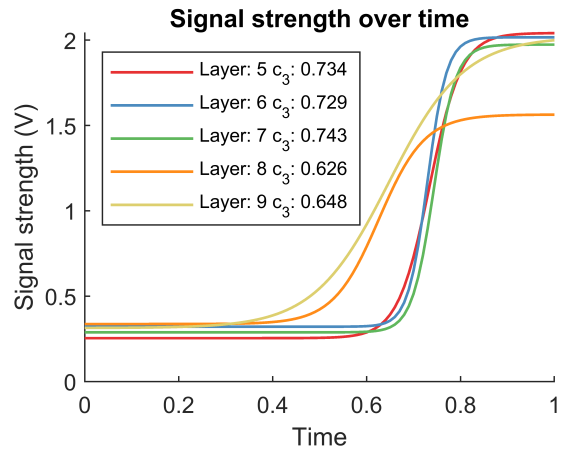
Appendix A

Appendix ice growth rate experiment

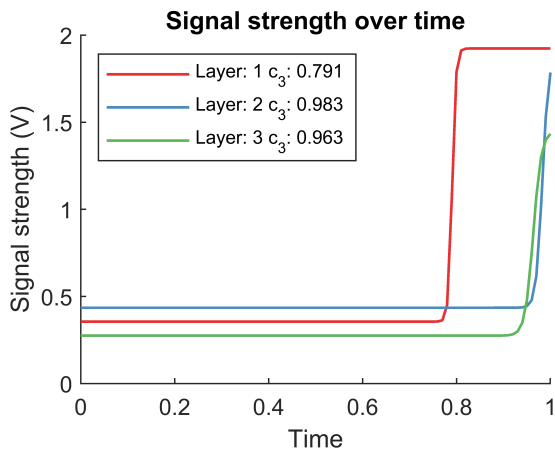
A.1 Ice growth experiment sigmoid curves



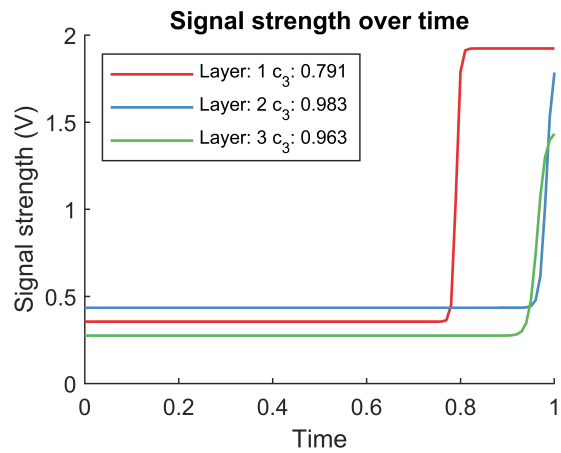
(a) One hour per layer.



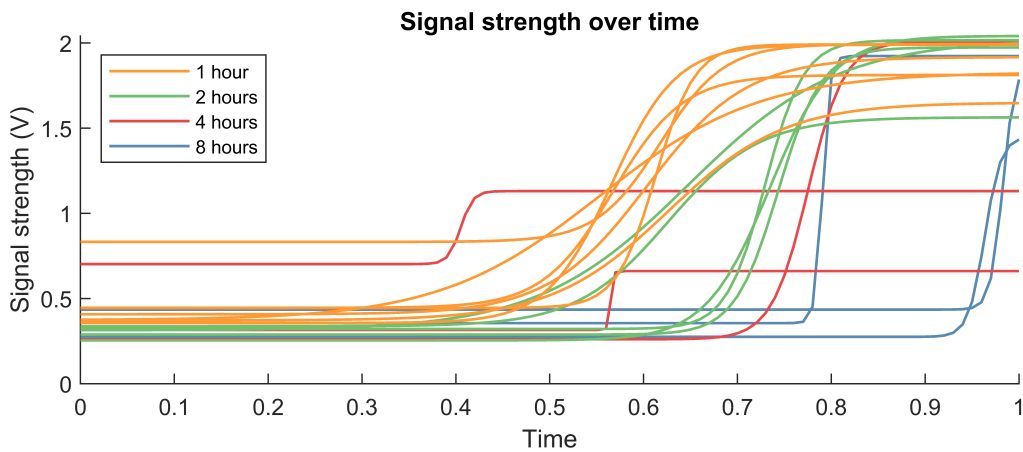
(b) Two hours per layer.



(c) Four hours per layer.



(d) Eight hours per layer.



(e) All different layer timings combined.

Figure A.1: Signal strength over time for a variety of layer duration's.

Appendix B

Material properties

B.1 Thermo-physical properties of pavement materials

Table B.1: Data for thermo-physical properties of pavement materials in dry state[28][21]

Specimen	ρ (kg m ⁻³)	λ (W m ⁻¹ K)	C_p (J kg K)	a (10×10^7 m ² s ⁻¹)
Plain concrete	1600-3000	0.50-5.00	800-1200	1.4-20.8
Sub-soil	1400-2000	0.30-2.00	800-1100	1.4-17.8
Crushed gravel/hardcore	2190-2403	1.10	1000	4.6-5.0
Soil-aggregate mix	1650	1.00	960	6.3

Appendix C

Spray cart design

C.1 Water layer height spray cart

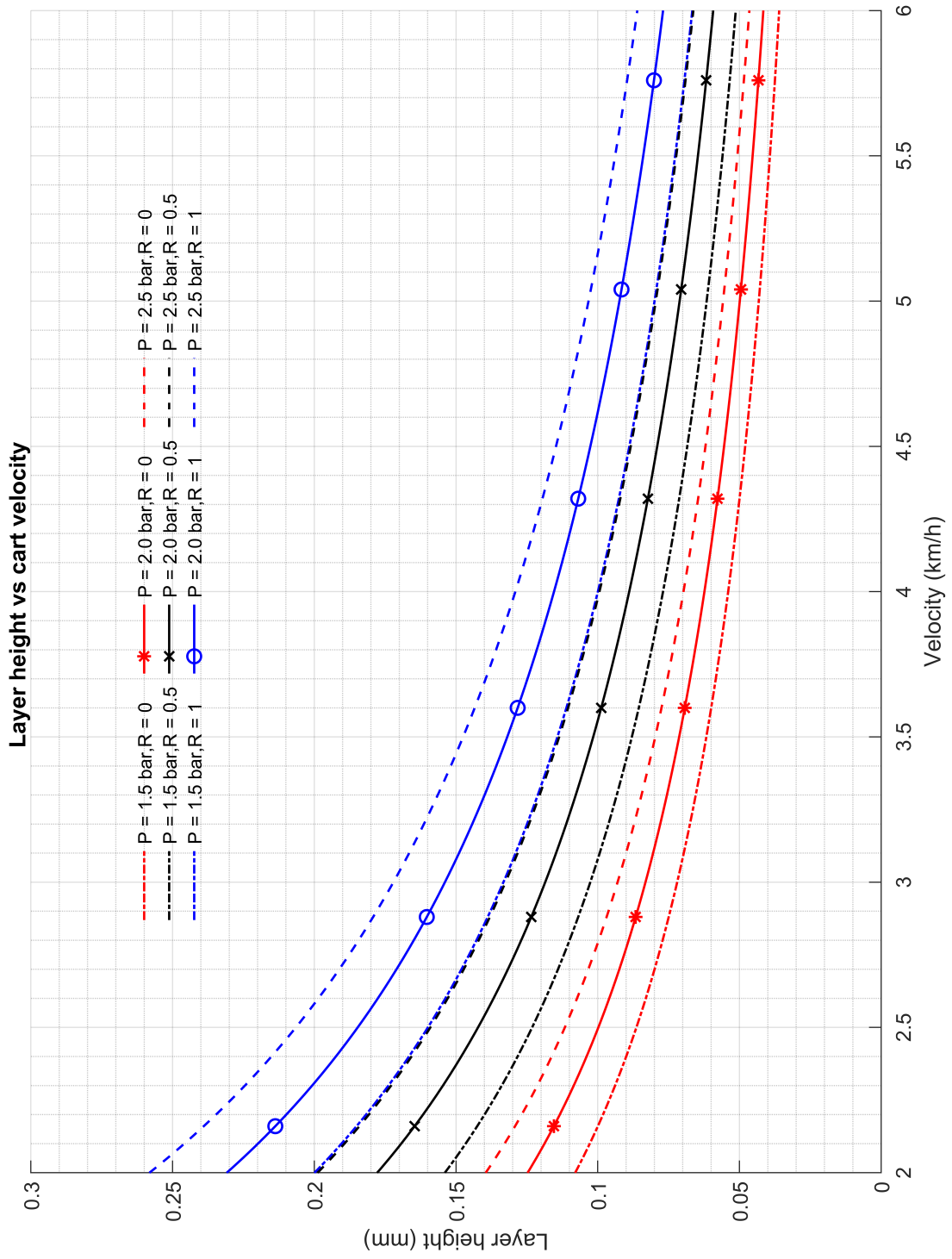


Figure C.1: On the y-axis water layer height and on the x-axis cart velocity. Using three distinct nozzle ratios and three different pressures.